Distribution and Mobility of Platinum-Group Elements in the Late Cretaceous Ni-laterite in the Northern Oman Mountains

Salah A. Al-Khirbash[a+] and Ahmed H. Ahmed[b,c]

[a] Department of Earth Sciences, Sultan Qaboos University, Muscat, Oman

[b] Faculty of Earth Science, King Abdulaziz University, Jeddah 21589, Saudi Arabia

[c] Department of Geology, Faculty of Science, Helwan University, Cairo, Egypt

[+]corresponding author: S. Al-Khirbash (khirbash@squ.edu.om)

Abstract

Low-grade Ni-laterite deposits are well-developed over the mafic/ultramafic protoliths in the northern Oman Mountains. Concentrations, distribution patterns and mobility of platinum-group element (PGE) are investigated in some Ni-laterite profiles of the Oman ophiolite as a possible unconventional PGE resource. The ultramafic protolith displays the lowest PGE content (average total PGE = 35 ppb), which is almost similar to the PGE content in the overlying saprolite zone. The PGE content substantially increased upward in the laterite profile, where the highest total PGE content (up to 253 ppb) is recorded in the oxide and ferricrete/clay-rich zones. The highest PGE content corresponds to Pt > Ru > Pd, while the lowest PGE content is mostly corresponding to Os < Rh < Ir, There is a general positive correlation between PGE contents and both Cr_2O_3 and Fe_2O_3 contents in the Ni-laterite profiles. This may reflect the formation of PGE-Fe nanoparticle alloys that are hosted by Fe-rich oxyhydroxides or due to the residual accumulation of chromite in the oxide and ferricrete/clay-rich zones during the lateritization process. The PGE distribution patterns and positive correlation with the ultramafic index of alteration (UMIA) indicate that PGE can be mobilized in different proportions in the surficial environment upon progressive lateritization processes. The high concentration of total PGE in the Oman Ni-laterite is in good agreement with

the PGE-rich laterite deposits worldwide, which can be considered as an unconventional PGE resource if adequate extraction and refining processes can be applied for their recovery from the possible upcoming Ni production.

Keywords: Ni-laterite, platinum-group elements (PGE), ultramafic index of alteration (UMIA), Oman ophiolite

1. Introduction

Platinum-group elements (PGE) are considered among the so-called critical metals which are essential for the high technological industry. However, the conventional PGE deposits (e.g., stratiform chromitite and magmatic sulfide deposits) from which these metals can be extracted are very limited in the world. The oxidation and supergene enrichment process, also known as the lateritization process, is chemical weathering resulting in the dissolution, transportation, and redistribution of various elements at or near the Earth's surface. Laterite profiles produced by pervasive chemical weathering of mafic/ultramafic rocks were known to be an important source of metallic deposits such as nickel (Ni), cobalt (Co), and iron (Fe), which are known in literature as Ni-laterites (Evans, 1993; Freyssinet et al., 2005; Golightly, 2010; Thorne et al., 2012a, 2012b; Butt & Cluzel, 2013; Reich & Vasconcelos, 2015). Supergene enrichment process is also one of the important processes for residual and secondary enrichment of PGE and gold in these mineral deposits (Bowles et al., 1994; Gray et al., 1996; Varajão et al., 2000; Traoré et al., 2008; Aiglsperger et al., 2015, 2016, 2017; Rivera et al., 2018; Tobón et al., 2020). There is a consensus that three main processes are possibly controlling the PGE concentration and distribution in terrestrial rocks. They are partial melting, crystal fractionation, and post-magmatic alteration (Barnes et al., 1985). Platinum (Pt) and gold (Au) are more mobile than the other PGE during the weathering processes, while palladium (Pd) might be mobilized by hydrothermal fluids (e.g., Keays et al., 1981, 1982; Barnes et al., 1985; Stumpfl, 1986). Some Ni-laterite deposits show unexpectedly high total PGE contents (~ 4 ppm) such as those in the Acoje (Philippines) and Musongati and Kapalagulu (Burundi) laterites (Bandyayera, 1997), which can be used as unconventional PGE resource. These may add values to the lateritization processes as a potential agent for PGE accumulation via chemical weathering of mafic/ultramafic rocks. Despite that, the effect of lateritization on PGE enrichment and platinum-group minerals (PGM) accumulation is

still a matter of debate. In some places, PGE-rich (about 3 ppm) with accumulation of various types of PGM have been previously reported from Ni-laterites in the Falcondo laterite deposit of the Dominican Republic, which might be attributed to the presence of small chromitite pods associated with serpentinized dunite (Proenza et al., 2007; Zaccarini et al., 2009; Proenza et al., 2010; Aiglsperger et al., 2015). Although the Ir-subgroup (IPGE = Os, Ir, and Ru) is considered to be highly resistant compared to the Pd-subgroup (PPGE = Rh, Pt, and Pd) under surficial conditions, several authors recognized that IPGE can also be mobilized under hydrothermal and/or lateritic weathering conditions (Stockman & Hlava, 1984; Garuti & Zaccarini, 1999; Zaccarini et al., 2005; Garuti et al., 2007, 2012). The lateritization process occasionally produces secondary PGE alloys, sulfides, sulfarsenides, and/or oxides/hydroxides by alteration of primary magmatic PGM precursors (Cornelius et al., 2008; Ndjigui & Bilong, 2010). However, supergene formation of PGM without the presence of magmatic PGM precursors has previously been reported from the platiniferous Au-Pd belt of Minas Gerais of Brazil (e.g. Cabral et al., 2009, 2011).

The Oman ophiolite represents one of the best-preserved oceanic lithospheres in the world, where a complete sequence of ophiolite stratigraphy is well-preserved and exposed from the upper mantle to the upper crust. The mantle sequence of the Oman ophiolite is essentially composed of tectonized harzburgite with minor dunites, lherzolites, and chromitites (Roberts, 1986). The mineralogical classification and general chemical characteristics of some Ni-laterite profiles from the northern mountains of the Oman ophiolite were previously studied to characterize the mineralization zones and their economic importance (Al-Khirbash, 2015, 2016, 2020; Al-Khirbash et al., 2014). The chromitite deposits of the Oman ophiolite were found to contain high content of PGE (Ahmed & Arai, 2002) and various types of PGM, which mainly comprised IPGE sulfides and, to a lesser extent, sulfarsenides (Ahmed & Arai, 2003). Oxidation of primary PGM sulfides into oxides is also described at low temperature conditions in the Oman ophiolitic chromitites (Ahmed et al., 2002). Desulfurization/oxidation is the main process in the surface environment that is responsible for the transformation of primary PGE sulfides into oxides and PGE-Fe alloys. To constrain the PGE distribution patterns, mobility, and concentration in supergene environments, their distribution in the Ni-laterite of the Oman ophiolite is analyzed in the present research. In this contribution, a detailed bulk-rock analysis and PGE geochemistry from six different Ni-laterite profiles of the Northern Oman Mountains is thoroughly studied with the aim

to understand the behavior, distribution, and mobility of PGE in the oxidation and supergene environments. A comparison with world-class laterite deposits is also done to assess the economic potentiality of the PGE in the Oman Ni-laterites.

2. Geologic settings

The present study is located at about 180 km SW of Muscat and lies around Saqah town between N 22^{o} 45` and $22^{o}$ 50` and 58^{o} 40` $58^{o}$ 50` (Figure 1a). The area is covered by the Late Cretaceous allochthonous ultramafic/mafic rocks of the Semail ophiolite nappe that was emplaced as a result of the obduction of the Tethyan rocks onto Middle Permian to Middle Cretaceous shelf carbonate sequences of the Arabian passive continental margin (Glennie et al., 1974; Coleman, 1981; Boudier et al., 1985; Dercourt et al., 1986; Lippard et al., 1986; Skelton et al., 1990; Searle & Cox, 2002; Peters et al., 2005; Searle, 2019). Small outcrops exposed on the eastern part of the study area consist of the deep marine limestone, radiolarian chert, and pelagic sediments (Hawasina window) and low-grade epidote greenschist facies metasedimentary rocks, cherts, marbles, and quartzites (metamorphic sole) (Cowan et al., 2014) (Figure 1b).

The Ni-laterites from the Northern Oman Mountains are part of the Maastrichtian neo-autochthonous post-obduction terrigenous clastic facies (Qahlah Formation) and lie unconformably on the obducted Semail ophiolite while they are capped by post-obduction Late Campanian/Maastrichian–Tertiary sedimentary rocks of the Simsima formation (Abbasi et al., 2014). The presence or absence of the laterite in the Northern Oman Mountains might reflect the original irregular paleotopography, the existence of basins associated with syn-sedimentary structures, and the prevailing climatic conditions at the end of the Cretaceous period that all initiated an intense and prolonged weathering process of the ophiolite (Nahon et al., 1982; Nolan et al., 1990; Al-Khirbash et al., 2010).

This work is based on field work and mineralogical and physical characteristics of laterite from six localities (1 to 6) in the Northern Oman Mountains (Figure 1). Localities 3 and 4 were combined in one profile as they logged along two sides of the road cut. The studied laterite profiles can be grouped into two main zones: the protolith zone and the laterite zone (Figure 2). The protolith consists of either relatively unweathered layered gabbro or serpentinized peridotite in the

most localities (Figures 2, 3a, 3b). The laterite zone comprises the in-situ green to grayish saprolite horizon, the reddish to brown massive to pisolitic oxide horizon, and the upper ferricrite or in some localities the compact clay-rich horizon (Figures 2, 3c, d, e, f).

The presence of protolith relics within the saprolite zone, gradual changes of element distribution (from the protolith to the upper zones), and the survival of chromian spinel and Cr-rich magnetite within the laterite zones, are all reflect in-situ development of laterite materials in the northern Oman Mountains. A detailed field and mineralogical description of these zones was given by Al-Khirbash (2015, 2016).

3. Sampling and analytical techniques

Twenty-nine samples were collected from six lateritic profiles in the Oman Mountains (six from the protolith, 4 from the saprolite zone, 15 from the oxide zone, 4 from the clay/ferricrite zone) for PGE and Au analyses (Figure 2). Samples were selected based on the mineralogical and geochemical characteristics of previous studies (Al-Khirbash, 2015, 2016), particularly those that showed high content of Cr-Ni-Co. The rock samples were broken into small chips using a hydraulic rock splitter and then pulverized using a Fritsch Pulverisette 5 planetary mill for 30 to 45 minutes. Samples up to 60 g in size were assayed using a nickel sulfide (NiS) fire assay Neutron Activation Analysis (INAA) procedure. The nickel sulfide were dissolved in concentrated HCl, and the resulting residue, which contains all the PGE and Au were collected on a filter paper. The residue underwent two irradiations and three separate counts to measure all the PGE and Au. One batch of analyses consists of the 29 samples in addition to two blanks, three certified standards, and three duplicates. Detection limits were as follows: Os (2 ppb), Ir (0.1 ppb), Ru (5 ppb), Rh (0.2 ppb), Pt (0.5 ppb), Pd (2 ppb), and Au (0.5 ppb). All analyses were carried out at Activation Laboratories Ltd. (Ancaster, Ontario, Canada).

Thin sections were prepared and subsequently investigated under transmitted optical microscopy. Selected samples from different laterite zones were examined with a PANalytical X'Pert PRO X-ray diffractometer with Cu λ Kα=1.54060 Å, a Ni Filter at 40 kV and 45 mA. The XRD patterns were recorded at a time step of 0.4 s for 2θ varies from 5° to 70°. The XRD analyses

were carried out at the Central Analytical and Applied Research Unit (CAARU) Sultan Qaboos University (Oman).

4. Petrography

Microscopic studies of the protoliths showed that the layered gabbro consists of fresh to altered plagioclase crystals with some altered pyroxenes (Figure 4a), and the serpentinized peridotites consist of pyroxene crystals that are altered to lizardite and chrysotile (Figure 4b). The above saprolite horizon comprises compact gray-greenish color rocks with abundant light-green lizardite and chrysotile minerals and commonly contains carbonate-filled fractures (Figure 4c). The oxide horizon is predominantly composed of hematite and goethite with rounded and ellipsoidal pisolite appearance (Figure 4d). The upper ferricrite/ironstone horizon consists mainly of massive hematite, goethite with magnetite, and inherited chromite grains that are replaced by hematite and authigenic chlorite (Figures 4d, e). XRD data confirmed the presence of these minerals (Figure 5).

5. Geochemistry

5.1 Major and compatible trace element geochemistry

Based on mineralogical characteristics as well as variations in physical properties such as texture, structure, and color, the laterite profiles of the Oman ophiolite can be classified into four categories: (1) protolith, which is represented by serpentinized peridotites and layered gabbros; (2) saprolite, which is the partly weathered zone overlying the protolith; (3) oxide zone, and (4) the ferricrete/clayrich zone, which represents the uppermost part of the laterite profiles. Geochemically, there are slight differences in major and compatible trace elements contents between the protolith and saprolite zones. Thus, they will deal together in the following descriptions, however they are clearly discriminated in figures and tables. On the other hand, the oxide and ferricrete/clayrich zones show significant geochemical differences compared with the protolith and saprolite zones. The major and selected compatible trace (Cr, Ni, Co) elements compositions of the protolith, saprolite, and oxide, and ferricrete/clayrich zones of the studied laterite profiles are shown in Tables 1 and 2.

5.1.1 Protolith and saprolite zones

The Ni-laterite profiles of the Oman Mountains are well-developed over serpentinized peridotites and/or over layered gabbros (Figure 2). The serpentinization process of ultramafic rocks adds water into the system, where serpentinized peridotites can contain more than 13 wt.% of water in the produced hydrous mineral crystal structure (e.g., Deschamps et al., 2013). However, a careful description of the samples should be done because the loss on ignition (LOI) is not always correlated with the degree of serpentinization since the presence of other hydrous phases such as talc, brucite, chlorite, and clay minerals can influence this budget. Careful petrographic investigation and X-ray diffraction (XRD) analysis of the studied serpentinized peridotite protolith of the Oman laterite profiles confirm the absence of such hydrous minerals, except the lizardite, antigorite, and clinochrysotile that represent the major mineral phases in the studied serpentinized peridotite protolith (Figure 5) (Al-Khirbash, 2016). The peridotite protolith of all laterite profiles shows the same compositional ranges in terms of their LOI and major and compatible trace elements constituents. The LOI of the peridotite protolith varies from 14.72 wt.% to 16.18 wt.%, with an average of 15.43 wt.% (Table 1). The low CaO content (0.05–2.82 wt.%, with an average of 0.97 wt.%) in the serpentinized peridotites reveals that serpentinization is the only process affecting the peridotite protolith. The LOI in the saprolite zone shows comparable values to the underlying serpentinized peridotites, varying from 14.59 wt.% to 15.88 wt.%, with an average of 15.27 wt.%, and a similar range of CaO content (Table 1). The common major oxides (SiO_2, MgO, Fe_2O_3, and Al_2O_3) do not show significant differences between the peridotite protolith and the overlying sparolite zone, where the average contents of these components are 37.23 wt.%, 36.08 wt.%, 7.78 wt.%, and 1.16 wt.%, respectively, in the former and 38.32 wt.%, 35.17 wt.%, 8.23 wt.%, and 0.79 wt.%, respectively, in the latter (Table 1). The most compatible trace elements (e.g., Cr_2O_3, NiO, Co_3O_4, and MnO) show comparable values in both the saprolite zone and the underlying peridotite protolith. The average NiO content in the saprolite zone (0.26 wt.%) is relatively higher than those in the underlying peridotite protolith (0.18 wt.%) (Table 1). The Cr_2O_3 and MnO contents are almost similar in the peridotite protolith and in the saprolite zone. They are averaging 0.38 wt.%, 0.36 wt.%, and 0.13, 0.11 wt.%, respectively (Table 1).

5.1.2 Oxide and ferricrete/clayrich zones

The upper oxide and ferricrete/clay-rich zones of the laterite profiles show significant differences in terms of the LOI, major constituents, and compatible trace elements compared with their protolith and saprolite zones. In terms of the major constituents, the distinguishing feature of these uppermost parts of the laterite profiles is the substantial increase in Fe_2O_3 and Al_2O_3 contents and the extreme leaching of SiO_2 and MgO compared with the underlying protolith and saprolite zones. The oxide and ferricrete/clayrich zones of the studied laterite profiles show comparable data of wide compositional ranges in terms of their major and compatible trace element constituents. SiO_2 is the most prominent component that is progressively decreased from the protolith to the uppermost oxide and ferricrete/clayrich zones. It displays reverse correlation with both total iron, as Fe_2O_3, and Al_2O_3 contents (Figures 6a, b). The SiO_2 content varies from 27.06 wt.% in the less lateritized samples down to 2.23 wt.% in the strongly lateritized ones (Table 2). The total iron, as Fe_2O_3, is highly increased with the increasing degree of lateritization. It varies from 31.14 ti 85.50 wt.% and from 16.82 to 78.18 wt.% in the oxide and ferricrete/clay-rich zones, respectively (Figure 6a). The Al_2O_3 content shows the highest value in the ferricrete/clay-rich zone, where it reaches up to 24.49 wt.%, and the lowest Al_2O_3 value (1.70 wt.%) is reported in the oxide zone (Figure 6b). MgO, on the other hand, is the most leachable component in the oxide and ferricrete/clay-rich zones of the laterite profiles. It is decreased to 0.40 and 0.37 wt.% in the highly lateritized samples of the oxide and ferricrete/clay-rich zones, respectively (Figures 6c, d). The MgO content shows strong positive and negative correlations, respectively, with SiO_2 (Figure 6c) and Fe_2O_3 (Figure 6d). In terms of the compatible trace elements (Cr, Ni, Co, and Mn), they are highly (Cr and Ni) to slightly (Co and Mn) enriched in the oxide and ferricrete/clay-rich zones of the laterite profiles compared with the protolith and saprolite zones (Table 2). Cr_2O_3 is the most enriched compatible component in the uppermost oxide and ferricrete/clay-rich zone, where it reaches up to 5.35 wt.% (3.36 wt.% average) and 11.44 wt.% (5.47 wt.% average) in the two laterite zones, respectively (Table 2). Similarly, the NiO content in the oxide and ferricrete/clay-rich zones of the laterite profiles reaches up to 2.85 wt.% (1.11 wt.% average) in oxide zone, and up to 2.01 wt.% (0.70 wt.% average) in the ferricrete/clay-rich zone. It is highly enriched in the oxide zone (up to 11 times greater than the Ni content in the protolith) and in the ferricrete/clay-rich zone (up to 8 times greater than the Ni content in the protolith). NiO content is generally increased with increasing Fe_2O_3 and Al_2O_3 contents (Table 2 and Figure 7a). The Co_3O_4 and MnO contents also relatively increase in the oxide and ferricrete/clay-rich zones, which reach up to 0.50 wt.% and 2.52 wt.%,

respectively (0.11 wt.% and 0.36 wt.% on average), showing a good positive correlation with NiO and Fe_2O_3 contents (Table 2).

5.2 Platinum-group elements (PGE) geochemistry

5.2.1 Protolith and saprolite zones

The PGE contents in the serpentinized peridotite and the saprolite zones in all profiles are similar, with very limited variations (Table 1). The total PGE content of the serpentinized peridotite protolith ranges between 20 and 36 ppb (31 ppb on average), which shows approximately flat chondrite-normalized PGE distribution patterns (Figure 9a) with slight positive fractionation ratios (average Pd/Ir_N and Ru/Pt_N = 1.54 and 0.99, respectively). It is noteworthy that the total IPGE (= Os, Ir, and Ru) is progressively increased along with the increase of PPGE (= Rh, Pt, and Pd) from the protolith to the saprolite and then to the oxide and ferricrete/clay-rich zones of the laterite profiles (Figure 8). The saprolite samples of laterite profiles show relative enrichment in total PGE compared with the serpentinized peridotites, varying from 36 to 93 ppb (58 ppb on average), which is mostly showing flat PGE distribution patterns, but sometimes with pronounced positive trend from Os to Ru then flat from Rh to Pd (Table 1 and Figure 9b). The Pd/Ir_N and Ru/Pt_N fractionation ratios reflect the relative enrichment in the IPGE compared with the PPGE. The average Pd/Ir_N and Ru/Pt_N ratios in the saprolite samples are 1.93 and 1.43, respectively. The Au content in the peridotite protolith and saprolite zones is approximately similar, which varies from 1 upto 5 ppb (Table 1).

5.2.2 Oxide and ferricrete/*clay-rich zones*

The total PGE content in the oxide and ferricrete/clay-rich zones of the laterite profiles is very high compared with those in the protolith and saprolite zones. The enrichment factor reaches up to six times in the oxide and ferricrete/clay-rich zones. Total PGE content varies from 59 up to 253 ppb (139 ppb on average) in the oxide zone, and from 43 to 176 ppb (107 ppb on average) in the ferricrete/clay-rich zone (Table 2). Both IPGE and PPGE sub-groups are substantially increased in the oxide and ferricrete/clay-rich zone of the laterite profiles, showing a general positive trend from Os to Pd in the chondrite-normalized PGE distribution patterns (Figures 9c, d). There is an obvious enrichment in the total PGE contents, with promotion of the lateritization process from the protolith upward to the uppermost oxide and ferricrete/clay-rich zones, which is reflected by

the substantial increase in Fe_2O_3, Cr_2O_3, and NiO contents (Figures 7b–d). The Pd/Ir_N and Ru/Pt_N ratios also reflect the general increase in both IPGE and PPGE in the PGE distribution patterns, which vary respectively from 0.45 to 3.81 (1.43 on average) and from 0.51 to 7.75 (2.78 on average) in the oxide and ferricrete/clay-rich zones. The ∑IPGE/∑PPGE ratio varies from 0.3 to 0.86 (0.61 on average) in the peridotite protolith, from 0.52 to 2.11 (1.12 on average) in the saprolite, and from 0.31 to 2.18 (1.16 on average) in the oxide/ ferricrete/clay-rich zone. There is a clear progressive increase of both IPGE and PPGE contents upward from the protolith to the oxidized zone of the laterite profiles (Figure 8). The Au content in the oxide and ferricrete/clay-rich zones is relatively higher than those in the protolith and saprolite zones. It reaches up to 15 ppb in the ferricrete/clay-rich zone (Table 2).

6. Discussion

6.1 Degree of lateritization

When the mafic/ultramafic rocks are exposed to the surface, they undergo intense chemical and mechanical weathering processes, which are mainly controlled by climatic and topographic conditions (Golightly, 1981, 2010; Freyssinet et al., 2005). These oxidation and supergene processes lead to the leaching of major elements (i.e., MgO and SiO_2) from the ferromagnesian minerals (olivine and pyroxenes) in parent rocks, whereas other elements (e.g., Ni, Mn, and Co) can be enriched up to ~~the~~ economic values (Aiglsperger et al., 2016). Water-insoluble oxides ~~metals~~ such as Fe_2O_3, Al_2O_3, and Cr_2O_3 are also residually accumulated in situ as oxides and oxyhydroxides, which play an important role as metals-retention phases in the uppermost part of the laterite profiles (Butt ~~&~~ & Cluzel, 2013; Bowles et al., 2017). To evaluate the degree of lateritization and chemical changes in ultramafic rocks during the formation of Ni-laterite, Aiglsperger et al. (2016) defined a factor called ultramafic index of alteration (UMIA), which is mainly based on the index of lateritization (IOL) proposed by Babechuk et al. (2014). The UMIA is calculated using the molar ratios of the major element oxides from the wt.% contents of the whole rock analysis (Duzgoren-Aydin et al., 2002), and the IOL is calculated as the wt.% of the major oxides (Babechuk et al., 2014; Aiglsperger et al., 2016; Tupaz et al., 2020). The following equations are used to calculate the UMIA and IOL:

$$UMIA = 100 \times [(Al_2O_3 + Fe_2O_{3(T)})/(SiO_2 + MgO + Al_2O_3 + Fe_2O_{3(T)})]$$

$$IOL = 100 \times [(Al_2O_3 + Fe_2O_{3(T)})/(SiO_2 + MgO + Fe_2O_{3(T)})]$$

These weathering indexes depend on the composition of ultramafic rocks (i.e., peridotites) that are essentially dominated by MgO and SiO_2, with negligible amounts of CaO, Na_2O, and K_2O (Babechuk et al., 2014). The breakdown of primary minerals is occasionally followed by the development of secondary minerals such as serpentine, chlorite, clay minerals, and oxyhydroxide phases (e.g., Fe-Mn oxides and hydroxides) (Rivera et al., 2018). Thus, the values of UMIA and IOL indexes give important information about the weathering trend of ultramafic rocks, which can also be shown as ternary diagrams of A-SM-F [(Al_2O_3-(SiO_2+MgO)-Fe_2O_3] and AF-S-M [(Al_2O_3+Fe_2O_3)-SiO_2-MgO] (Figures 10a, b), and the IOL is shown as ternary S-A-F (SiO_2-Al_2O_3-Fe_2O_3) ternary diagram (Figure 10c). The UMIA of the ultramafic protolith of the Oman Ni-laterite ranges from 3% to 5%, with an average of 4%, and the less weathered saprolite samples are more or less similar to the underlying protolith where the values of UMIA vary from 3% to 4% (Figure 10a). The oxide and ferricrete/clay-rich zones of the laterite profiles have UMIA values between 38% and 88% (69% on average) in the oxide zone, and from 39 – 89% (73% on average) in the ferricrete/clay-rich zone (Table 2, Figures 10a, b). The IOL, on the other hand, is comparable with the UMIA values, where the average values in the protolith, saprolite, oxide and ferricrete/clay-rich zones are 4%, 4%, 78% and 84%, respectively (Figures 10a–c). Except one sample from locality #1 where the Al_2O_3 content is exceptionally high, the Ni-laterite profiles of the Oman ophiolite are characterized by constantly high Fe/Al ratios (Figures 10a–c and Table 2). It is obvious that both Al_2O_3 and Fe_2O_3 contents are progressively increased with the increasing degree of lateritization (i.e., UMIA) toward the surface of the laterite profiles. There is a good direct relationship between the two components, from the ultramafic protolith to the oxide and ferricrete/clay-rich zones (Figure 11a). The Ni and Co, which are mainly hosted by ferromagnesian minerals (e.g., olivine and pyroxenes) in the parent rocks, are also progressively increased with the increasing degree of lateritization (Figure 11b), as concluded by Al-Khirbash (2016), and are hosted by goethite, chlorite, kaolinite, and other Ni-bearing serpentine and talc (Al-Khirbash 2015). The residual accumulation of chromite in the uppermost part of laterite profiles is also obvious, which clearly increases with the increasing process of lateritization (Figure 11c). This is also clearly shown by the enrichment of total PGE with the increase in Cr_2O_3 contents in the laterite profiles. This is because chromite is considered as one of the main hosts of PGE in general and IPGE in particular (Table 2). Based on the calculated UMIA and IOL values, the Oman Ni-

laterite are in a good agreement with the moderately lateritized profiles worldwide (Babechuk et al., 2014; Rivera et al., 2018).

6.2 PGE enrichment in Ni-laterite

In general, the total PGE contents in Ni-laterites around the world are ranging between ≤ 100 ppb and up to few hundreds ppb in content (Augé & Legendre, 1994; Eliopoulos & Economou-Eliopoulos, 2000; Ndjigui & Bilong, 2010; Aiglsperger et al., 2015, 2016; Rivera et al., 2018). However, in some places, exceptionally enriched lateritic crusts with 2 ppm, as well as more than 4 ppm total PGE, were reported in the Ora Banda Sill in Western Australia (Gray et al., 1996) and in Burundi (Maier et al., 2008). In all of the studied Ni-laterite profiles from the Northern Oman Mountains, the uppermost oxide and ferricrete/clay-rich zones show the highest PGE contents compared with the saprolitic zone and the underlying protolith. The anomalous concentration of PGE contents in the upper levels of the weathering profile, compared with their initial low contents in the underlying bedrocks, as well as the positive correlation between the UMIA and total PGE contents (Figure 11d), indicate that PGE can be mobilized in different proportions throughout the weathering profile (e.g., Aiglsperger et al., 2016; Rivera et al., 2018; Tobón et al., 2020). From the PGE distribution patterns (Figures 9a–d), it is clearly shown that Ru, Pt, and Pd are more mobile than Ir and Rh, while Os shows the highest mobility in the surficial environment where it is mostly leached out from the weathered profiles. The pronounced Ru positive anomalies from all of the studied laterite profiles are mostly attributed to its presence as laurite (RuS_2) crystals, or as Ru-Fe alloys, within the residually accumulated chromite grains in the weathered laterite profiles. Although PGM grains were not reported from the studied Ni-laterite profiles (it needs more careful observations under high magnifications), it is confirmed from previous studies on the Oman ophiolite where the main PGE mineralogy are laurite in the primary chromite (Ahmed & Arai, 2003) and PGE oxides in weathered lithologies (Ahmed et al., 2002). The residual accumulation of chromite grains (represented by high Cr_2O_3 content) in the oxide and ferricrete/clay-rich zones compared with the Cr_2O_3 content in the protolith and saprolite zones (Fig. 7c) (at least 10 to 15 times greater than the protolith content), can substantially contribute to the high Ru content. The PGE mobility in surficial environments can be attributed to the lateritization processes that resulted in the migration of these metals toward the oxide and oxyhydroxide zones (Eliopoulos & Economou-Eliopoulos, 2000; Talovina & Lazarenkov, 2001; Ndjigui & Bilong, 2010; Aiglsperger

et al., 2015). The PGE mobility and redistribution within the laterite profile are most probably controlling by: (1) the Eh–pH ratio of the weathering solutions, (2) the Cl concentration in the laterite profile, and (3) the mode of occurrence of PGM in the parent rocks before weathering (Bowles et al., 1994a, 1994b; Salpéteur et al., 1995; Ahmed & Arai, 2002, 2003; Ahmed et al., 2002). In addition to the Pt-Pd-Cl complexes, the Pt and Pd as redox metals can also be mobilized as inorganic complexes in low temperature conditions (Colombo et al., 2008). The highly accumulated chromite grains in the uppermost part of the weathered profiles of the Oman ophiolite (Figure 11c) could be accompanied by the enrichment of total PGE, in general, and IPGE, in particular. The IPGE, which have higher melting points than the PPGE, tend to be concentrated in refractory phases (i.e., chromite) and in early cumulates relative to PPGE, which are more incompatible and tend to be retained in the residual melt and crystallized with the interstitial sulfide phase (Barnes et al., 1988; Edwards, 1990; Prichard et al., 1996a, 1996b). Thus, PPGE could be easily mobilized and redistributed during the chemical weathering of parent rocks than the IPGE, which are mainly related to the chromite accumulation. The available data, however, suggests that Os is amongst the most soluble PGEs under the surficial conditions, where it shows the lowest content in all of the studied laterite profiles. Both mechanisms, the leaching of PPGE from the interstitial sulfide phase and the accumulation of IPGE with chromite, will lead to the increase in both of them in the oxide and ferricrete/clay-rich zones of the laterite profiles (Figure 8).

Previous studies on the mobility of PGE during lateritization processes revealed that acidic conditions ($pH < 6$ and $Eh > 0.4$) could lead to the dissolution of PGE-bearing minerals, especially PPGE phases, and then they would undergo subsequent transportation in solution and accumulation in the oxidized Fe-rich laterite profiles (Plimer & Williams, 1988; Bowles et al., 1994a, 1994b; Talovina & Lazarenkov, 2001). The PGE are accumulated as PGE-rich alloys, which co-precipitate with Fe and Mn oxides under such acidic conditions (Bowles et al., 1994a, 1994b; Salpéteur et al., 1995; Ndjigui & Bilong, 2010; Tobón et al., 2020). Complex Pt-Ir-Fe-Ni alloys were recently found as inclusions and packed nanoparticles within pore spaces of Fe oxides and oxyhydroxides of the Loma Peguera Ni-laterite deposit in the Dominican Republic (Aiglsperger et al., 2015, 2017) and in the Planeta Rica Ni-laterite profiles of Northern Colombia (Tobón et al., 2020). These observations are in good agreement with the previous studies, which indicated that the high contents of Pt, Pd, and Ru, as well as the transition metals such as Ni, Co, Cu, and Zn, in laterite profiles, are essentially hosted by secondary minerals like Fe-oxy-

hydroxides or smectite clay minerals (Oberthür & Melcher, 2005; Ndjigui & Bilong, 2010). The high total PGE contents in the oxide and ferricrete/clay-rich zones of the Oman Ni-laterite profiles are in accordance with this idea and could be accumulated as PGE-Fe alloys that co-precipitated with oxides and oxyhydroxides. The newly formed supergene PGE alloys could be formed in situ during lateritization processes by dissolving the primary magmatic PGM precursor (Aiglsperger et al., 2016).

6.3 Possible economic potentiality

Although the total PGE contents (< 300 ppb) in the Ni-laterite profiles of the Oman ophiolite do not reach the economic values, they are mostly comparable to the total PGE contents reported from PGE-rich Ni-laterite profiles around the world, such as Ni-laterite deposits of Falcondo in the Dominican Republic, Cuba (Aiglsperger et al., 2015, 2016), and New Caledonia (Traoré et al., 2008); Ni-laterite from Centinela Bajo, south-central Chile (Rivera et al., 2018); and those from the Cerro Matoso and Planeta Rica Ni-Laterite deposits, Northern Colombia (Tobón et al., 2020). For example, the Ni-laterite deposit of Falcondo of the Dominican Republic has PGE values before processing between 250 and 640 ppb. However, the final product obtained after pyrometallurgical extraction shows an increase in total PGE contents up to 2 ppm (Aiglsperger et al., 2015, 2016). Similarly, in the Ni-laterite deposits of Cuba, the PGMs are mainly collected in the sulfide concentrates and the Ni-end products during the ore dressing in the Nikaro and Moa ore dressing plants, where the PGE contents reach up to 6 ppm (Lazarenkov et al., 2005). Such final PGE values are considered as a potential unconventional PGE resource from the Falcondo and Cuba Ni-laterite deposits.

In the Ni-laterite profiles of the Oman ophiolite, the PGE contents in the oxide and ferricrete/clay-rich zones reached up to 253 ppb (up to 6 magnitude as those in the parent ultramafic rocks), which is almost comparable to those reported from worldwide PGE-rich Ni-laterite deposits (Figure 12). The PGE enrichment in the oxide zone of the laterite profiles corresponds to an increase in NiO, Co_3O_4, Cr_2O_3, Fe_2O_3, and Al_2O_3 contents, as well as to the highest calculated degrees of lateritization (average UMIA ~70%) (Figures 11a–d). The formation of secondary nanoparticles of PGE alloys in the oxide and oxyhydroxide zones of the Oman laterite profiles needs more careful investigation using ultrahigh magnification tools such as the field emission scanning electron microscope (FESEM) and/or Raman spectroscopy techniques, which is beyond the scope

of this article. In addition, further field investigations and systematic sampling are needed to focus on the profiles having more concentration of Cr_2O_3 contents and progressive high degrees of lateritization. Although the PGE contents in the oxidized horizons of the Oman Ni-laterite profiles are not economic in its current natural form, applying adequate extraction and refining methods in the future could increase the PGE contents, which might be recovered as by-products. If it is applied in the future, the Ni laterite of the Oman ophiolite can be considered as unconventional PGE deposits.

6. Conclusions

1. The Ni-laterite profiles of the Oman ophiolite characterized by the progressive increase in Fe_2O_3 Al_2O_3, Cr_2O_3, NiO, and Co_3O_4 contents from parent ultramafic rocks to the oxide and ferricrete/clay-rich zones in the uppermost part of the laterite profile. This also corresponds to the strong leaching of SiO_2 and MgO contents from the oxidized zone of the laterite profiles.
2. The highest PGE contents in the Ni-laterite of the Oman ophiolite are concentrated in the oxide and ferricrete/clay-rich zones, which reached up to six times as their contents in the saprolite and peridotite protolith. The PGE distribution patterns and positive correlation of total PGE contents with the UMIA, as well as the increase of Cr_2O_3 contents in the oxide and ferricrete/clay-rich zones of laterite profiles, indicate that the PGE can be mobilized in different proportions.
3. Ru, Pt, and Pd are more mobile than Os, Ir, and Rh. The positive correlation between IPGE and PPGE with the increasing degree of lateritization is indicative of their mobilization, redistribution, and enrichment in the Fe-rich oxides and oxyhydroxides of the laterite profiles. The IPGE are most probably, at least partly, linked with the residual accumulation of chromite in the oxide and ferricrete/clay-rich zones, while the PPGE are most probably leached from the interstitial sulfides.
4. The PGE contents of the Oman Ni-laterite are in accordance with the PGE values from the worldwide Ni-laterite deposits. It can be considered as an unconventional PGE resource if adequate extraction and refining processes are applied to increase the PGE contents in the final products.
5. Further field investigations focusing on the Ni-laterite profiles with high degrees of lateritization and those enriched in Cr_2O_3 contents are needed to check the existence of PGE

enrichment in these laterite profiles. A detailed mineralogical study using ultrahigh magnification tools is also needed to identify the possible presence of PGE-Fe alloy nanoparticles in the oxide and oxyhydroxide zones of the Ni-laterites.

Acknowledgments

This research was funded by the SQU Deanship of Research (RF/SCI/ETHS/20/01). We appreciate the Department of Earth Sciences and the Central Analytical Applied Research Unit (CAARU) for allowing us to use their analytical facilities. Dataset supports this research is from Al-Khirbash, S.A. (2016). Geology, mineralogy, and geochemistry of low grade Ni-lateritic (Oman Mountains, Oman). *Chemie der Erde, 76(3),* 363–381. https://doi.org/10.1016/j.chemer.2016.08.002.

The authors declare that there is no conflict of interest.

References

Abbasi, I.A., Salad Hersi, O., & Al-Harthy A. (2014). Late Cretaceous post-obduction conglomerates of the Qahlah Formation, north Oman: Depositional system and implications for basin configuration. In: H.R Rollinson., M.P. Searle, I.A. Abbasi, A. Al-Lazki, & M.H. Al Kindi (eds.). Tectonic Evolution of the Oman Mountains: *Geol. Soc. Spec. Publ., 392(1),* 325–341. DOI: 10.1144/SP392.17

Ahmed, A., & Arai, S. (2002). Unexpectedly high-PGE chromitite from the deeper mantle section of the northern Oman ophiolite and its tectonic implications. *Contributions to Mineralogy and Petrology, 143***,** 263–278. https://doi.org/10.1007/s00410-002-0347-8.

Ahmed, A., & Arai, S. (2003). Platinum-group minerals in podiform chromitities of the Oman ophiolite. *The Canadian Mineralogist, 41 (3),* 597–616.doi: https://doi.org/10.2113/gscanmin.41.3.597.

Ahmed, A.H., Arai, S. & Kadoshima, K. (2002). Possible platinum-group element (PGE) oxides in the PGE-mineralized chromitite from the northern Oman ophiolite. *Journal of Mineralogical and Petrological Sciences, 97*, 190-198. https://doi.org/10.2465/jmps.97.190

Aiglsperger, T., Proenza, J.A., Zaccarini, F., Lewis, J.F., Garuti, G., Labrador, M., & Longo, F. (2015). Platinum group minerals (PGM) in the Falcondo Ni laterite deposit, Loma Caribe

peridotite (Dominican Republic). *Mineralium Deposita, 50,* 105-123. https://doi.org/10.1007/s00126-014-0520-

Aiglsperger, T., Proenza, J.A., Lewis, J.F., Labrador, M., Svojtka, M., Rojas-Purón, A., Longo, F. & Ďurišová, J. (2016). Critical metals (REE, Sc, PGE) in Ni laterites from Cuba and the Dominican Republic. *Ore Geology Review, 73,* 127-147. https://doi.org/10.1016/j.oregeorev.2015.10.010

Aiglsperger, T., Proenza, JA., Font-Bardia, M, Baurier-Aymat, S., Galí, S., Lewis, J.F., & Longo, F. (2017). Supergene neoformation of Pt-Ir-Fe-Ni alloys: multistage grains explain nugget formation in Ni-laterites. *Mineralium Deposita, 52,* 1069–1083. https://doi.org/10.1007/s00126-016-0692-6.

Al-Khirbash, S., Nasir, S., Al-Harthy, A., Richard, L., Al-Sayigh, A., Darkel, A., & Semhi, K. (2010). Geology and Ni-Co mineralization of laterites of the Oman Mountains, 7th International Symposium on the Eastern Mediterranean Geology, 18–22 October. Cukurova University, Adana.

Al-Khirbash, S. (2015). Genesis and Mineralogical Classification of Ni-laterites, Oman Mountains. *Ore Geology Reviews, 65,* 199–212. https://doi.org/10.1016/j.oregeorev.2014.09.022

Al-Khirbash, S.A. (2016). Geology, mineralogy, and geochemistry of low grade Ni-lateritic soil (Oman Mountains, Oman). *Chemie der Erde, 76(3),* 363–381. https://doi.org/10.1016/j.chemer.2016.08.002

Al-Khirbash, S. (2020). Mineralogical characterization of low-grade nickel laterites from the North Oman Mountains: Using mineral liberation analyses – scanning electron microscopy-based automated quantitative mineralogy. *Ore Geology Review, 120*. https://doi.org/10.1016/j.oregeorev.2020.103429

Al-Khirbash, S., Semhi, K., Richard, L., Nasir, S., & Al-Harthy, A.R. (2014). Rare earth element mobility during laterization of the mafic rocks of the Oman Mountains. *Arab Journal Geoscience, 7,* 5443-5454. 10.1007/s12517-013-1189-6.

Augé, T., & Legendre, O. (1994). Platinum-group element oxides form the pirogues ophiolitic mineralization, New Caledonia: Origin and significance. *Economic Geology, 89,* 1454-1468. https://doi.org/10.2113/gsecongeo.89.7.1454

Babechuk, M.G., Kamber, B.S., & Widdowson, M. (2014). Quantifying chemical weathering intensity and trace element release from two contrasting basalt profiles, Deccan Traps, India. *Chemical Geology, 363,* 56-75. https://doi.org/10.1016/j.chemgeo.2013.10.027

Bandyayera, D. (1997). Formation de laterites nickeliferes et mode de distribution des elements du groupe du platine dans les profils lateritiques du complexe de Musongati, Burundi (Ph.D. Thesis). Universite du Quebec a Chicoutimi, 440 pp. 10.1522/1531842

Barnes, S.J., Naldrett, A.J., & Gorton, M.P. (1985). The origin of the fractionation of platinum-group elements in terrestrial magmas. *Chemical Geology, 53,* 3O3-323. https://doi.org/10.1016/0009-2541(85)90076-2

Barnes, S.J., Boyd, R., Korneliussen, A., Nilsson, L.P., Often, M., Pedersen, R.B., & Robins, B. (1988). The use of mantle normalization and metal ratios in discriminating between the effects of partial melting, crustal fractionation and sulphide segregation on platinum group elements, gold, nickel and copper: Examples from Norway. In H.M. Prichard, P.J. Potts, J.F.W. Bowles, & S.J. Cribbs (eds.). *Geoplatinum-87: London, Elsevier, Applied Science,* pp. 113–143.

Bowles, J.F.W., Gize, A.P., & Cowden, A. (1994a). The mobility of the Platinum-Group elements in the soils of the Freetown peninsula, Sierra Leone. *Canadian Mineralogist, 32,* 957-967.

Bowles, J.F.W., Gize, A.P., Vaughan, D.J., & Norris, S.J. (1994b). The development of Platinum-Group Minerals in latérites; inorganic and organic controls. Transactions of the Institution of Mining and Metallurgy, Section B: *Applied Earth Science, 103,* 53-56

Bowles, J.F.W., Suárez, S., Prichard, H.M., & Fisher, P.C. (2017). Weathering of PGE sulfides and Pt–Fe alloys in the Freetown Layered Complex, Sierra Leone. *Minerlium Deposita, 52,* 1127–1144. https://doi.org/10.1007/s00126-016-0706-4

Butt, C., & Cluzel, D. (2013). Nickel Laterite Ore Deposits: Weathered Serpentinites. *Elements, 9(2),* 123-128. https://doi.org/10.2113/gselements.9.2.123

Cabral, A.R., Lehmann, B., Tupinambá, M., Schlosser, S., Kwitko-Ribeiro, R., & De Abreu, F.R. (2009). The platiniferous Au-Pd belt of Minas Gerais, Brazil, and genesis of its botryoidal Pt-Pd aggregates. *Economic Geology, 104(8),* 1265–1276. https://doi.org/10.2113/gsecongeo.104.8.1265

Cabral, A.R., Radtke, M., Munnik, F., Lehmann, B., Reinholz, U., Riesemeier, H., Tupinambá, M., & Kwitko-Ribeiro, R. (2011). Iodine in alluvial platinum-palladium nuggets: evidence for

biogenic precious-metal fixation. *Chemical Geology, 281(1-2),* 152–132. https://doi.org/10.1016/j.chemgeo.2010.12.003

Colombo, C., Oated, C.J., Monhemius, A.J., & Plant, J.A. (2008). Complexation of platinum, palladium and rhodium with inorganic ligands in the environment. *Geochemistry: Exploration, Environment, Analysis, 8,* 91–101. https://doi.org/10.1144/1467-7873/07-151

Cornelius, M., Robertson, I.D.M., Cornelius, A.J., & Morris, P.A. (2008). Geochemical mapping of the deeply weathered western Yilgarn craton of Western Australia using laterite geochemistry. *Geochemistry: Exploration, Environment, Analysis, 8(3-4),* 241-254. https://doi.org/10.1144/1467-7873/08-172

Cowan, R. J., Searle, M. P., & Waters, D. J. (2014). Structure of the metamorphic sole to the Oman Ophiolite, Sumeini Window and Wadi Tayyin: implications for ophiolite obduction processes. *Geological Society, London, Special Publications, 392,* 155-175. https://doi.org/10.1144/SP392.8

Duzgoren-Aydin, N.S., Aydin, A., & Malpas, J. (2002). Distribution of clay minerals along a weathered pyroclastic rock profile, Hong Kong. *Catena, 50(1),* 17-41. https://doi.org/10.1016/S0341-8162(02)00066-8

Edwards, S.J. (1990). Harzburgites and refractory melts in the Lewis Hills massif, Bay of Island ophiolite complex: the base-metals and precious-metals story. *Canadian Mineralogist, 28,* 537–552

Eliopoulos, D.G., & Economou-Eliopoulos, M. (2000). Geochemical and mineralogical characteristics of Fe–Ni- and bauxitic-laterite deposits of Greece. *Ore Geology Reviews, 16(1-2),* 41–58. https://doi.org/10.1016/S0169-1368(00)00003-2

Freyssinet, P., Butt, C.R.M., Morris, R.C., & Piantone, P. (2005). Ore-forming processes related to lateritic weathering. In J.W. Hedenquist, J. F. H. Thomson, R. J. Goldfarb, & J. P. Richards (eds.). *Economic Geology 100th Anniversary Volume*. https://doi.org/10.5382/AV100.21

Garuti, G., Zaccarini, F., Moloshag, V., & Alimov, V. (1999). Platinum-group minerals as indications of sulfur fugacity in ophiolitic upper mantle: an example from chromitites of the Ray-is ultramafic complex, Polar Urals, Russia. *Canadian Mineralogist, 37(5),* 1099-1115.

Garuti, G., Proenza, J.A., & Zaccarini, F. (2007). Distribution and mineralogy of platinum-group elements in altered chromitites of the Campo Formoso layered intrusion (Bahia State, Brazil):

control by magmatic and hydrothermal processes. *Mineralogy and Petrology, 89,* 159–188.10.1007/s00710-006-0141-9

Garuti, G., Zaccarini, F., Proenza, J.A., Thalhammer, O.A.R., & Angeli, N. (2012). Platinum-group minerals in chromitites of the Niquelândia layered intrusion (Central Goias, Brazil): their magmatic origin and low-temperature reworking during serpentinization and lateritic weathering. *Minerals, 2(4),* 365–384. https://doi.org/10.3390/min2040365

Golightly, J.P. (1981). Nickeliferous laterite deposits. *Economic Geology 75th Anniversary Volume,* 710–735.

Golightly, J.P. (2010). Progress in understanding the evolution of nickel laterites, *Society of Economic Geology, Special Publication, 15*, 451−486. https://doi.org/10.5382/SP.15.2.07

Gray, J.D., Schorin, K.H., & Butt, C.R.M. (1996). Mineral associations of platinum and palladium in lateritic regolith, Ora Banda Sill, Western Australia. *Journal of Geochemical Exploration, 57(1-3),* 245-255. https://doi.org/10.1016/S0375-6742(96)00040-4

Keays, R.R., Ross, J.R., & Woolrich, P. (1981). Precious metal sin volcanic peridotite-associated nickel sulfide deposits in Western Australia. II. Distribution within the ores and host rocks at Kambalda. *Economic Geology, 76,* 1645–1674.

Keays, R.R., Nickel, E.H., Groves, D.I., & McGoldrick, P.J. (1982). Iridium and palladium as discriminants of volcanic-exhalative hydrothermal and magmatic nickel sulfide mineralization. *Economic Geology, 77(6),* 1535–1547. https://doi.org/10.2113/gsecongeo.77.6.1535

Lazarenkov, V.G., Tikhomirov, B., Zhidkov, Y., & Talovina, V. (2005). Platinum group metals and gold in supergene nickel ores of the Moa and Nikaro deposits (Cuba). *Lithology and Mineral Resources, 40,* 521-527. https://doi.org/10.1007/s10987-005-0049-1

Maier, W.D., Barnes, S-J., Chinyepi, G., Barton, Jr.J.M., Eglington, B., & Setshedi, I. (2008). The composition of magmatic Ni–Cu–(PGE) sulfide deposits in the Tati and Selebi-Phikwe belts of eastern Botswana. *Minerlium Deposita, 43,* 37–60. I 10.1007/s00126-007-0143-5

Mattern, F., Scharf, A., Pu-Jun Wang, P.J., Callegari, I., Abbasi, A., Al-Wahaibi, S., Pracejus, B., & Scharf, K. (2020). Deformation of the Cambro-Ordovician Amdeh Formation (Members 1 and 2): Characteristics, Origins, and Stratigraphic Significance (Wadi Amdeh, Saih Hatat Dome, Oman Mountains). *Geosciences, 10 (2), 48.* https://doi.org/10.3390/geosciences10020048.

Ndjigui, P.D., & Bilong, P. (2010). Platinum-group elements in the serpentinite lateritic mantles of the Kongo–Nkamouna ultramafic massif (Lomié region, South-East Cameroon). *Journal of Geochemical Exploration,107(1),* 63-76. 10.1016/j.gexplo.2010.06.008.

Oberthür, T., & Melcher, F. (2005). PGE and PGM in the supergene environment: The Great Dyke, Zimbabwe, In J.E. Mungall (ed.), Exploration for platinum-group element deposits. Mineralogical Association of Canada, *Short Course Series, 35,* 97-112.

Plimer, I.R., & Willians, P.A. (1988). New mechanism for the mobilization of the Platinum Group Elements in the supergene zone. In H. M. Prichard, P. J. Potts, J. F. W. Bowles, S. J. Cribb (eds.), Geo-Platinum 87, *Elsevier Applied Science Publications, London, U.K.,* pp. 83–92. https://doi.org/10.1007/978-94-009-1353-0_9

Prichard, H.M., Lord, R.A., & Neary, C.R. (1996a). A model to explain the occurrence of platinum- and palladium-rich ophiolite complexes. London: *Journal of Geological Society, 153,* 323-328. https://doi.org/10.1144/gsjgs.153.2.0323

Prichard, H.M., Puchelt, H., Eckhardt, J-D., & Fisher, P.C. (1996b). Platinum-group element concentrations in mafic and ultramafic lithologies drilling from Hess Deep. In C. Me´vel, K. M. Gillis, J. F. Allan, & P. S. Meyer (eds.), *Proceedings of Ocean Drilling Program, Scientific Results, 147,* pp 77–90. 10.2973/odp.proc.sr.147.004.1996

Proenza, J.A., Zaccarini, F., Lewis, J., Longo, F., & Garuti, G. (2007). Chromian spinel composition and platinum-group mineral assemblage of PGE-rich Loma Peguera chromitites, Loma Caribe peridotite, Dominican Republic. *Canadian Mineralogist, 45,* 211-228.

Proenza, J.A., Roqué, J., Labrador, M., Galí, S., Tauler, E., Gallardo, T., Lewis, J. F., & Longo, F. (2010). Mineralogical composition and mineral chemistry of supergene cobalt ores from eastern Cuba and Dominican Republic Ni-laterite deposits, *20th general meeting of the IMA,* 21-27.

Reich, M., & Vasconcelos, P. (2015). Geological and economic significance of supergene upgrading of metals. *Elements, 11(5),* 305-310. https://doi.org/10.2113/gselements.11.5.305

Rivera, J., Reich, M., Schoenberg, R., González-Jiménez, J.M., Barra, F., Aiglsperger, T., Proenza, J.A., & Carretier, S. (2018). Platinum-group element and gold enrichment in soils monitored by chromium stable isotopes during weathering of ultramafic rocks. *Chemical Geology, 499,* 84-99. https://doi.org/10.1016/j.chemgeo.2018.09.008

Roberts, S. (1986). The role of igneous processes in the formation of ophiolitic chromitite (Ph.D. Thesis). Open University, Milton Keynes. https://ethos.bl.uk/OrderDetails.do?uin=uk.bl.ethos.374493

Salpéteur, I., Martel-Jantin, B., & Rakotomanana, D. (1995). Pt and Pd mobility in ferrallitic soils of the West Andriamena area (Madagascar). Evidence of a supergene origin of some Pt and Pd minerals. *Chronicle of mineral research and exploration, 520,* 27-45.

Searle, M.P., & Cox, J. (2002). Subduction zone metamorphism during formation and emplacement of the Semail ophiolite in the Oman Mountains. *Geological Magazine, 139(3),* 241-255. https://doi.org/10.1017/S0016756802006532

Searle M.P. (2019). Ophiolites and Regional Tectonics. In: Geology of the Oman Mountains, Eastern Arabia. GeoGuide. Springer, Cham. https://doi.org/10.1007/978-3-030-18453-7_4

Stockman, H.W., & Hlava, P.F. (1984). Platinum-group minerals in Alpine chromitites from southwestern Oregon. *Economic Geology, 79(3),* 491-508. https://doi.org/10.2113/gsecongeo.79.3.491

Stumpfl, E.F. (1986). Distribution, transport and concentration of platinum-group elements. In M. J. Gallagher, R. A. Ixer, C. R. Neary, & H. M. Prichard (eds.), Metallogeny of basic and ultrabasic rocks. Institute of Mining and Metallurgy Publications, London, pp 379–394. http://pascal-francis.inist.fr/vibad/index.php?action=getRecordDetail&idt=8819820

Talovina, I.V., & Lazarenkov, V.G. (2001). Distribution and genesis of platinum group minerals in nickel ores of the Sakhara and Elizavet deposits in the Urals. *Lithology and Mineral Resources, 36,* 116–122. https://doi.org/10.1023/A:1004870316406

Thorne, R., Roberts, S., & Herrington, R. (2012a). The formation and evolution of the Bitincke nickel laterite deposit, Albania. *Mineralium Deposita, 47(8),* 933–947. http://dx.doi.org/10.1007/s00126-012-0411-x

Thorne, R.L., Roberts, S., & Herrington, R. (2012b). Climate change and the formation of nickel laterite deposits. *Geology, 40(4),* 331–334. https://doi.org/10.1130/G32549.1

Traoré, D., Beauvais, A., Chabaux, F., Peiffert, C., Parisot, J.C., Ambrosi, J.P., & Colin, F. (2008). Chemical and physical transfers in an ultramafic rock weathering profile: part 1. Supergene dissolution of Pt-bearing chromite. *American Mineralogist, 93(1),* 22–30. https://doi.org/10.2138/am.2008.2605

Tobón, M., Weber, M., Proenza, J.A., Aiglsperger, T., Betancur, S., Farré-de-Pablo, J., Ramírez, C., & Pujol-Solà, N. (2020). Geochemistry of platinum-group elements (PGE) in Cerro Matoso and Planeta Rica Ni-laterite deposits, northern Colombia. Boletín de la Sociedad *Geológica Mexicana, 72(3),* A201219. http://dx.doi.org/10.18268/ BSGM2020v72n3a201219

Tupaz, C.A.J., Watanabe, Y., Sanematsu, K., Echigo, T., Arcilla, C., & Ferrer, C. (2020). Ni-Co Mineralization in the Intex Laterite Deposit, Mindoro, Philippines. *Minerals, 10(7),* 579. https://doi.org/10.3390/min10070579

Varajão, C.A.C., Colin, F., Vieillard, P., Melfi, A.J., & Nahon, D. (2000). Early weathering of palladium gold under lateritic conditions, Maquiné mine, Minas Gerais, Brazil. *Applied Geochemistry, 15(2),* 245–263. https://doi.org/10.1016/S0883-2927(99)00038-4

Zaccarini, F., Proenza, A.J., Ortega-Gutierrez, F., & Garuti, G. (2005). Platinum group minerals in ophiolitic chromitites from Tehuitzingo (Acatlan complex, southern Mexico): implications for post-magmatic modification. *Mineralogy and Petrology, 84,* 147-168. 10.1007/s00710-005-0075-7

Zaccarini, F., Proenza, J.A., Rudashevsky, N.S., Cabri, L.J., Garuti, G., Rudashevsky, V.N., Melgarejo, J.C., Lewis, J.F., Longo, F., Bakker, R., & Stanley, C.J. (2009). The Loma Peguera ophiolitic chromitite (Central Dominican Republic): a source of new platinum group minerals (PGM) species. *Neues Jahrbuch für Mineralogie Abhandlungen, Journal of Mineralogy and Geochemistry, 185(3),* 335-349. https://doi.org/10.1127/0077-7757/2009/0127

List of Figures

Figure 3: Field photographs of the laterite horizons in the study area: (a) massive layered gabbro protolith, locality #3; (b) general view of the peridotite protolith, locality #5; (c) saprolite horizon with less altered peridotite blocks, locality #4; (d) massive oxide horizon, locality #6; (e) pisolitic reddish color oxide horizon, locality #6; and (f) fined-grained compact clay horizon, locality #1

Figure 4: Photomicrographs of the protolith and laterite horizons: (a) fresh plagioclase (Pl) crystals and altered pyroxenes (Cpy) in layered gabbro, XPL, locality #3; (b) pyroxene (Cpy) crystals that are altered to lizardite (lz) and chrysotile (Ctl) in serpentinized peridotites, XPL, locality #2; (c) lizardite (lz) and chrysotile (Ctl) minerals cut by carbonate-filling (Cb) fracture in the saprolite horizon, XPL, locality #3; (d) hematite and goethite minerals with rounded chlorite-core (Chl) pisolites in the oxide horizon, XPL, locality #4; and (e) hematite (Hem) and goethite (Gth), with magnetite (Mag) and inherited chromite (Chr) grains and authigenic chlorite (Chl), reflected XPL, locality #1.

Figure 5: XRD pattern of the representative sample of some selected laterite horizons: (a) saprolite zone, locality # 2; (b) saprolite zone, locality #4; (c) oxide zone, locality #5; and (d) oxide zone, locality # 6. Minerals: Ctl = chrysotile, Nep = nepouite, Lz = lizardite, Cal = calcite, Hem = hematite, Mag = magnetite, Ilm = ilmenite, and Tr = trevorite.

Figure 6: Compositional binary variation diagrams of major oxides of the studied Ni-laterite of the Oman Mountains. a, b, and c are variations of SiO_2 vs. Fe_2O_3, Fe_2O_3, and MgO wt.%, and d is the variation of Fe_2O_3 vs. MgO wt.%.

Figure 7: Compositional variation diagrams of (a) NiO vs. Fe_2O_3 wt.%. b, c, and d are variations of total PGE (ppm) vs. Fe_2O_3, Cr_2O_3, and NiO wt.%, respectively.

Figure 8: Variation diagram of IPGE vs. PPGE of the studied Ni-laterite profiles.

Figure 9: a, b, c, and d are chondrite-normalized PGE distribution patterns of the studied Ni-laterite profiles of the Oman Mountains. Normalizing values are taken from Naldrett and Duke (1980; cf. 514, 540, 690, 200, 1,020, and 545 for Os, Ir, Ru, Rh, Pt, and Pd, respectively).

Figure 10: Ternary plots (in molar %) of Al–Fe–Mg–Si space showing the weathering trends of ultramafic rocks, defined as the ultramafic index of alteration (UMIA): (a) A–SM–F ternary plot illustrating the weathering trend with respect to Al_2O_3 enrichment or Fe_2O_3 enrichment. (b) AF–S–M ternary plot illustrating the general weathering trend of peridotites with the initial loss of MgO, followed by the loss of SiO_2 and concomitant enrichment of Al_2O_3 and Fe_2O_3. Ternary variation diagrams are from Aiglsperger et al. (2016). (c) Al_2O_3-Fe_2O_3-SiO_2 space shows the index of lateritization (IOL) in wt.% (after Rivera et al., 2018).

Figure 11: (a, b) Variation diagrams of Al_2O_3 vs. Fe_2O_3 wt.% and NiO vs. Co_3O_4 wt.% of the studied Ni-laterite profiles showing the lateritization trend from the protolith to the overlying saprolite and oxidized zones. (c) Variation diagram showing the enrichment of Cr_2O_3 with the increase of the ultramafic index of alteration (UMIA). (d) Variation diagram showing the enrichment of total PGE with the increase of the UMIA.

Figure 12: Chondrite-normalized PGE distribution patterns of the studied Ni-laterite profiles compared with the compositional fields from the Moa Bay and the Falcondo mining areas, including both the pre- and the post-processing materials of PGE contents. Normalization values from Naldrett and Duke (1980).

List of Tables

Table 1: Major, selected trace elements composition (wt.%) and PGE contents (ppb) of the protolith and saprolite samples of the studied Ni-laterite profiles of the Oman ophiolite.

Table 2: Major, selected trace elements composition (wt.%) and PGE contents of the oxide and ferricrete/clay-rich zone samples of the studied Ni-laterite profiles of the Oman ophiolite.

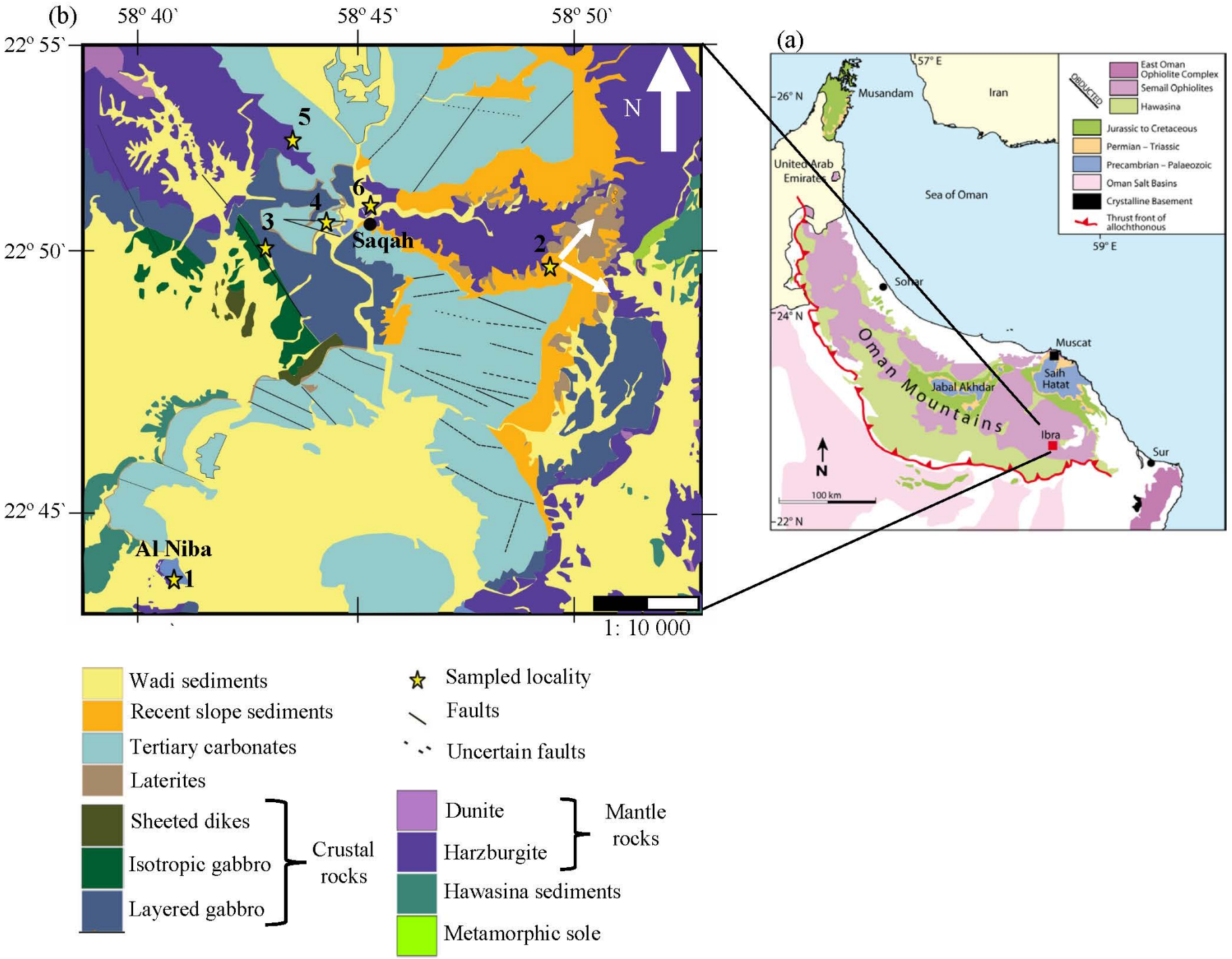
(b)
58° 40`
58° 45`
58° 50`
22° 55`
22° 50`
22° 45`
N
5
6
4
3
Saqah
2
Al Niba
1
1: 10 000
(a)
57° E
26° N
Musandam
Iran
United Arab Emirates
Sea of Oman
59° E
Sohar
24° N
Muscat
Saih Hatat
Jabal Akhdar
Oman Mountains
Ibra
Sur
N
100 km
22° N
East Oman Ophiolite Complex
Semail Ophiolites
Hawasina
OBDUCTED
Jurassic to Cretaceous
Permian – Triassic
Precambrian – Palaeozoic
Oman Salt Basins
Crystalline Basement
Thrust front of allochthonous
Wadi sediments
Recent slope sediments
Tertiary carbonates
Laterites
Sheeted dikes
Isotropic gabbro
Layered gabbro
Crustal rocks
Sampled locality
Faults
Uncertain faults
Dunite
Harzburgite
Mantle rocks
Hawasina sediments
Metamorphic sole

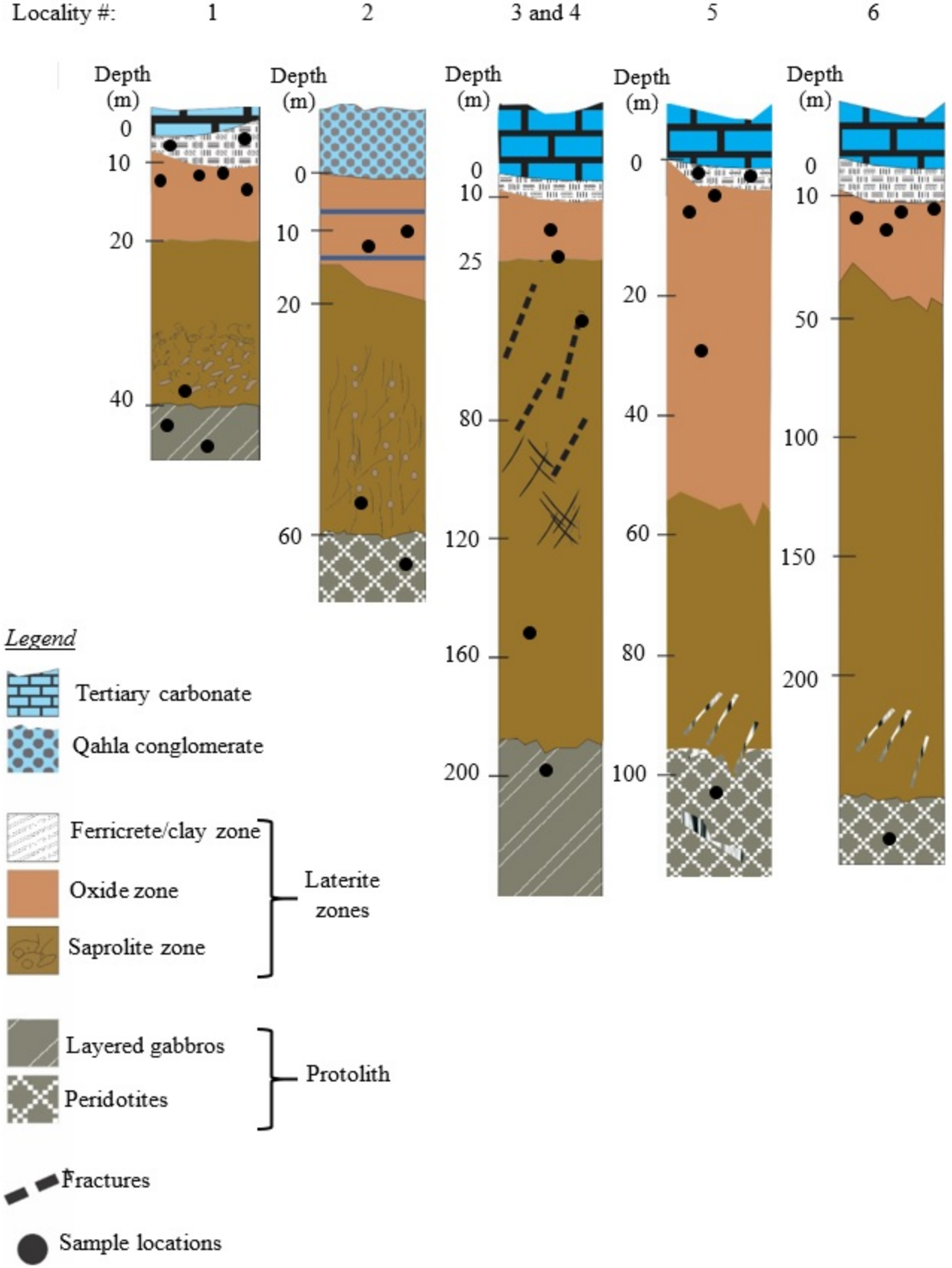
Locality #:
1
2
3 and 4
5
6
Depth (m)
0
10
20
40
Depth (m)
0
10
20
60
Depth (m)
0
10
25
80
120
160
200
Depth (m)
0
20
40
60
80
100
Depth (m)
0
10
50
100
150
200
Legend
Tertiary carbonate
Qahla conglomerate
Ferricrete/clay zone
Oxide zone
Saprolite zone
Laterite zones
Layered gabbros
Peridotites
Protolith
Fractures
Sample locations

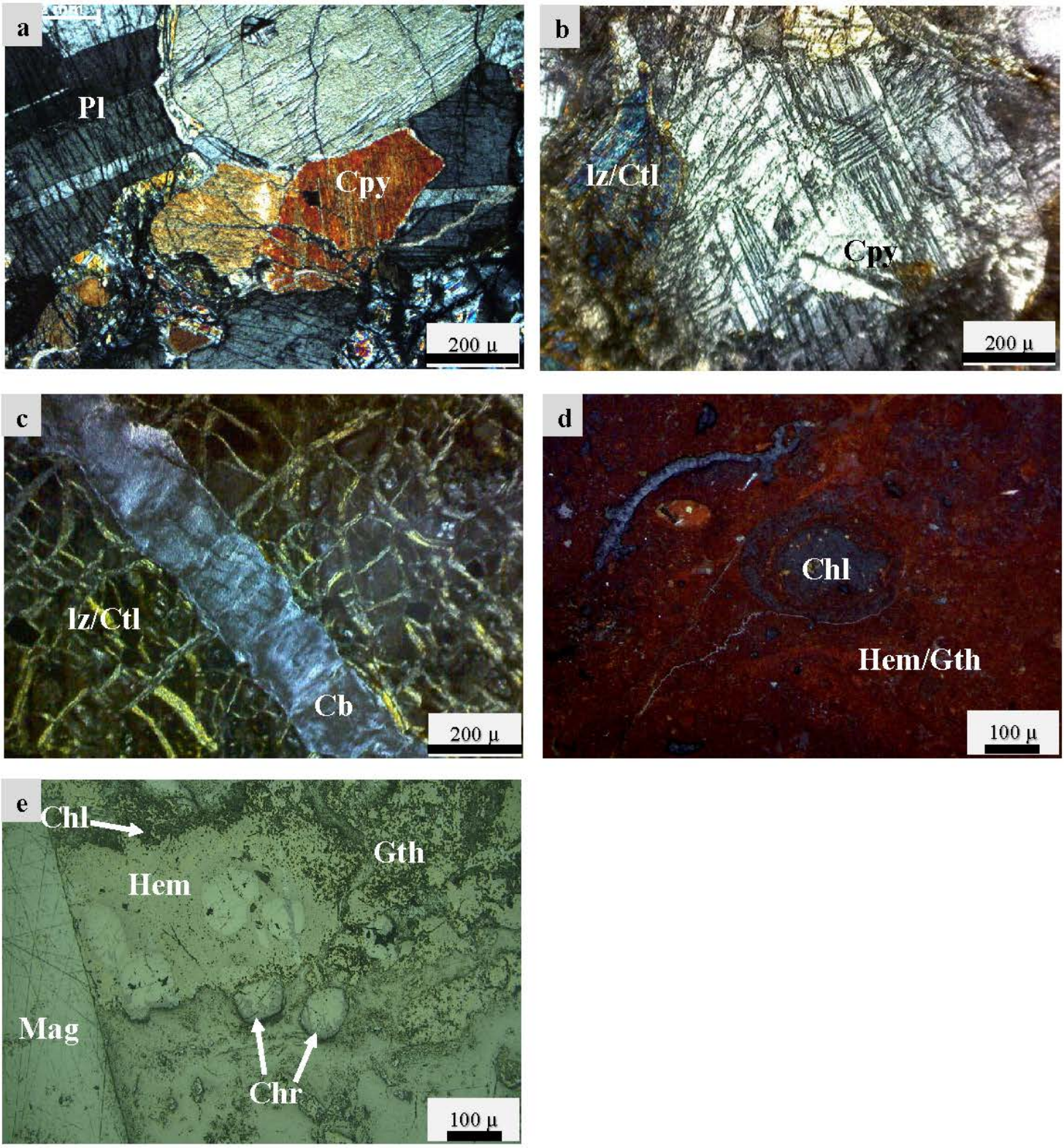
a
Pl
Cpy
200 µ
b
Iz/Ctl
Cpy
200 µ
c
Iz/Ctl
Cb
200 µ
d
Chl
Hem/Gth
100 µ
e
Chl
Gth
Hem
Mag
Chr
100 µ

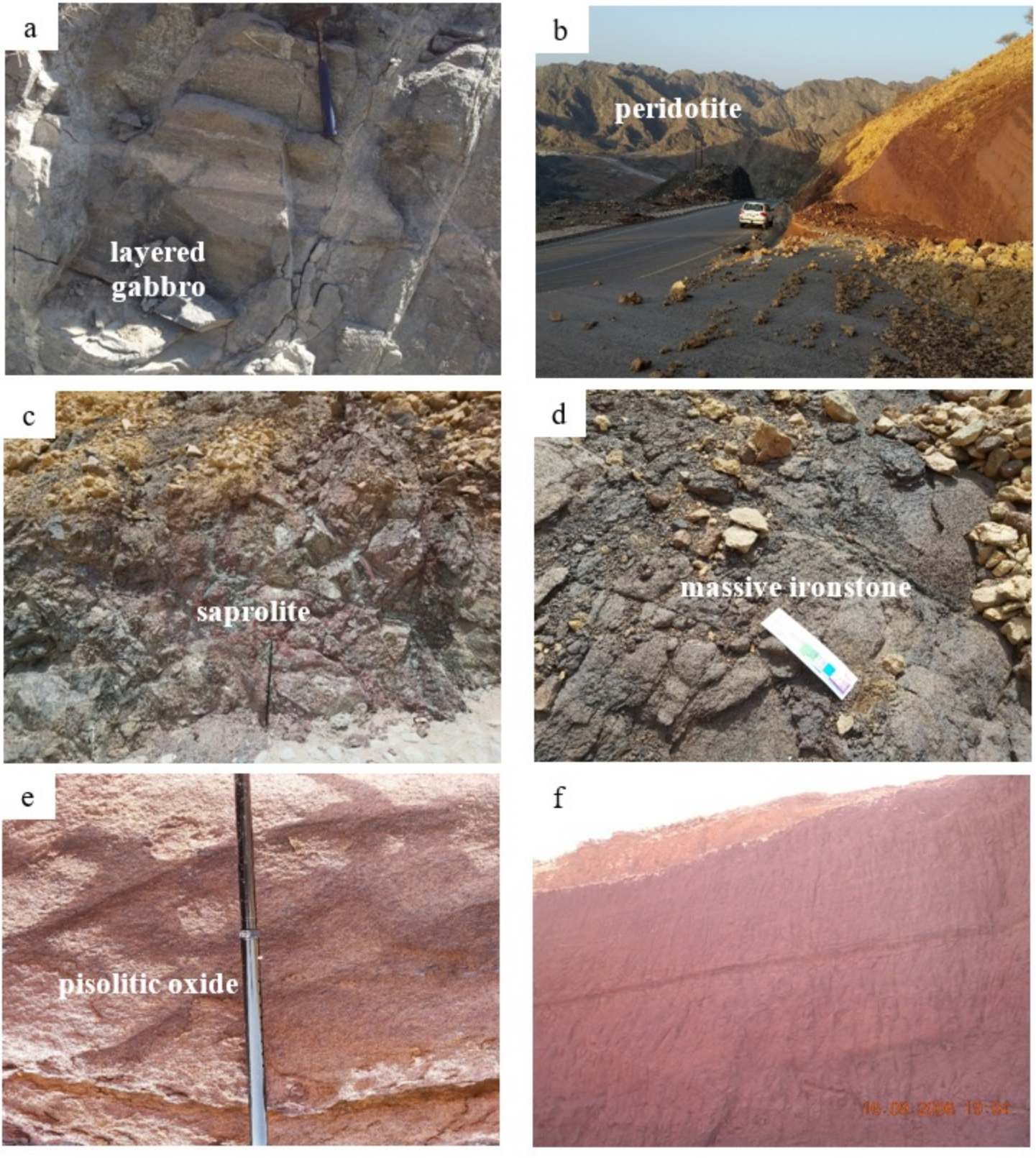
a
layered
gabbro
b
peridotite
c
saprolite
d
massive ironstone
e
pisolitic oxide
f

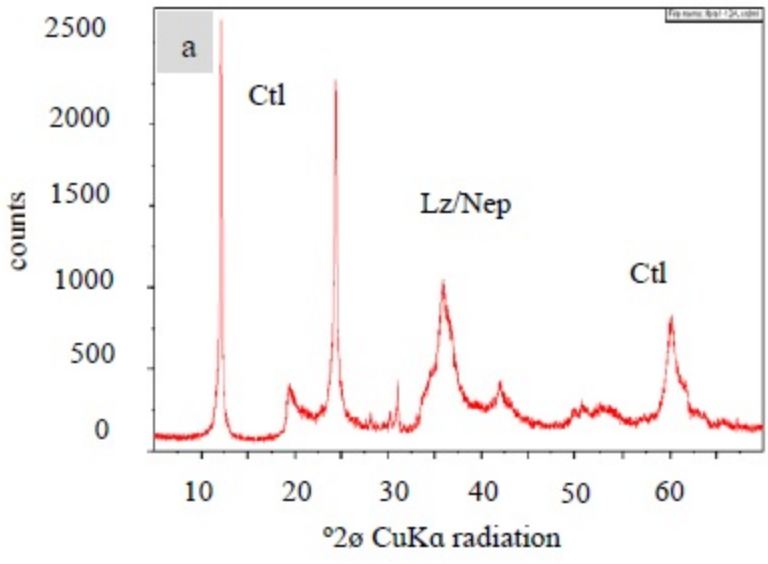
a
Ctl
Lz/Nep
Ctl
counts
2500
2000
1500
1000
500
0
10
20
30
40
50
60
°2ø CuKα radiation

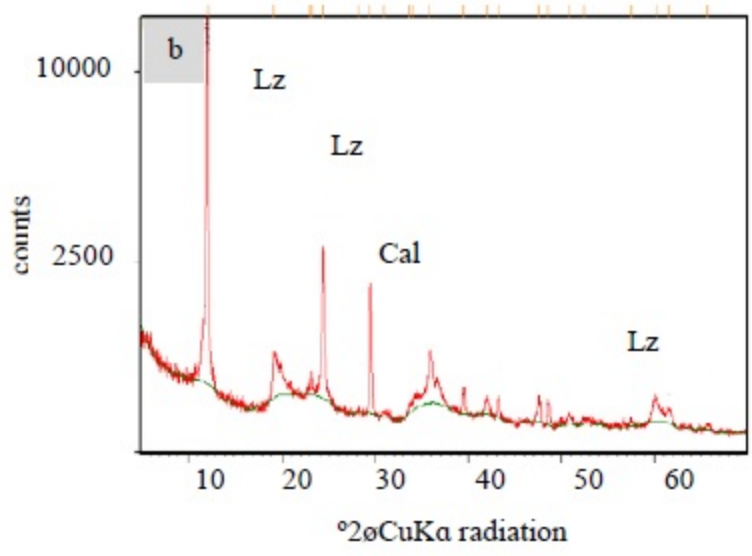
b
Lz
Lz
Cal
Lz
counts
10000
2500
10
20
30
40
50
60
°2øCuKα radiation

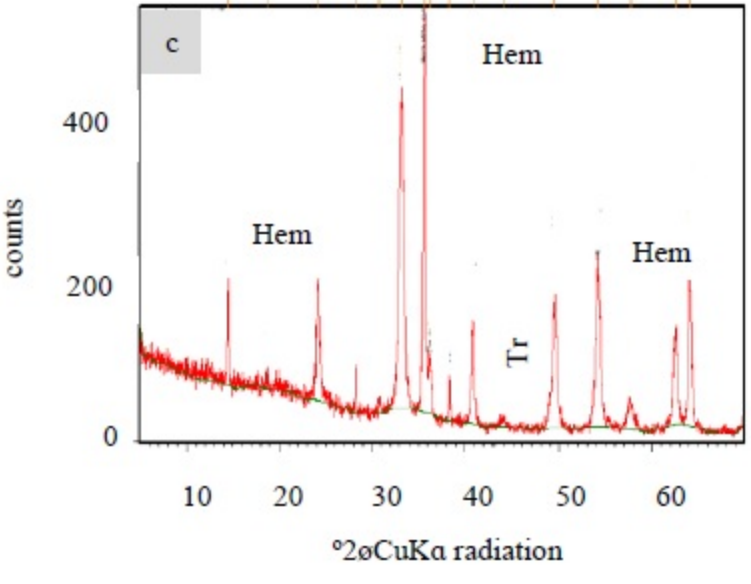
c
Hem
Hem
Hem
Tr
counts
400
200
0
10
20
30
40
50
60
°2øCuKα radiation

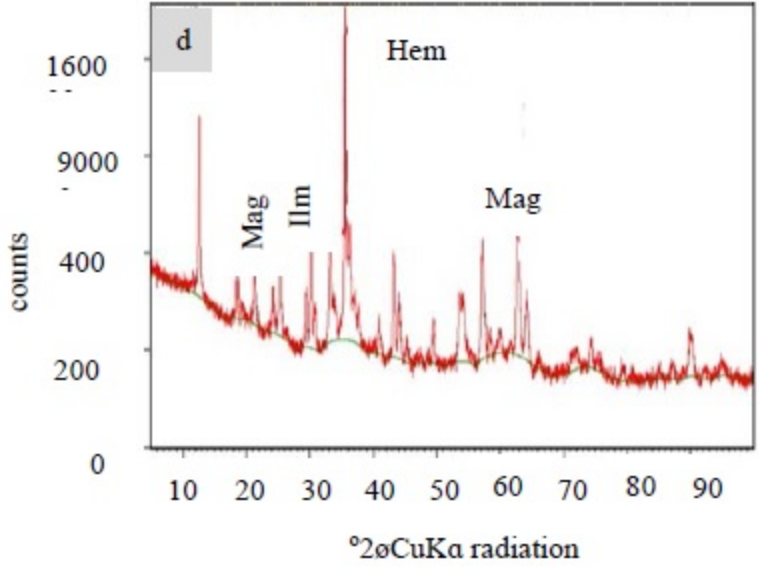
d
Hem
Mag
Ilm
Mag
counts
1600
9000
400
200
0
10
20
30
40
50
60
70
80
90
°2øCuKα radiation

(a)

Al_2O_3 wt.%

Lateritization trend

(b)

Fe_2O_3 wt.%

Lateritization trend

(c)

MgO wt.%

Lateritization trend

SiO_2 wt.%

(d)

MgO wt.%

Lateritization trend

SiO_2 wt.%

Fe_2O_3 wt.%

Ferricrete/clay-rich zone

Oxide zone

Saprolite

Protolith

(a)

NiO wt.%

Lateritization

(b)

Total PGE (ppb)

Lateritization

Fe_2O_3 wt.%

Ferricrete/clay-rich zone
Oxide zone
Saprolite
Protolith

(c)

Total PGE (ppb)

Lateritization

Cr_2O_3 wt.%

(d)

Total PGE (ppb)

Lateritization

NiO wt.%

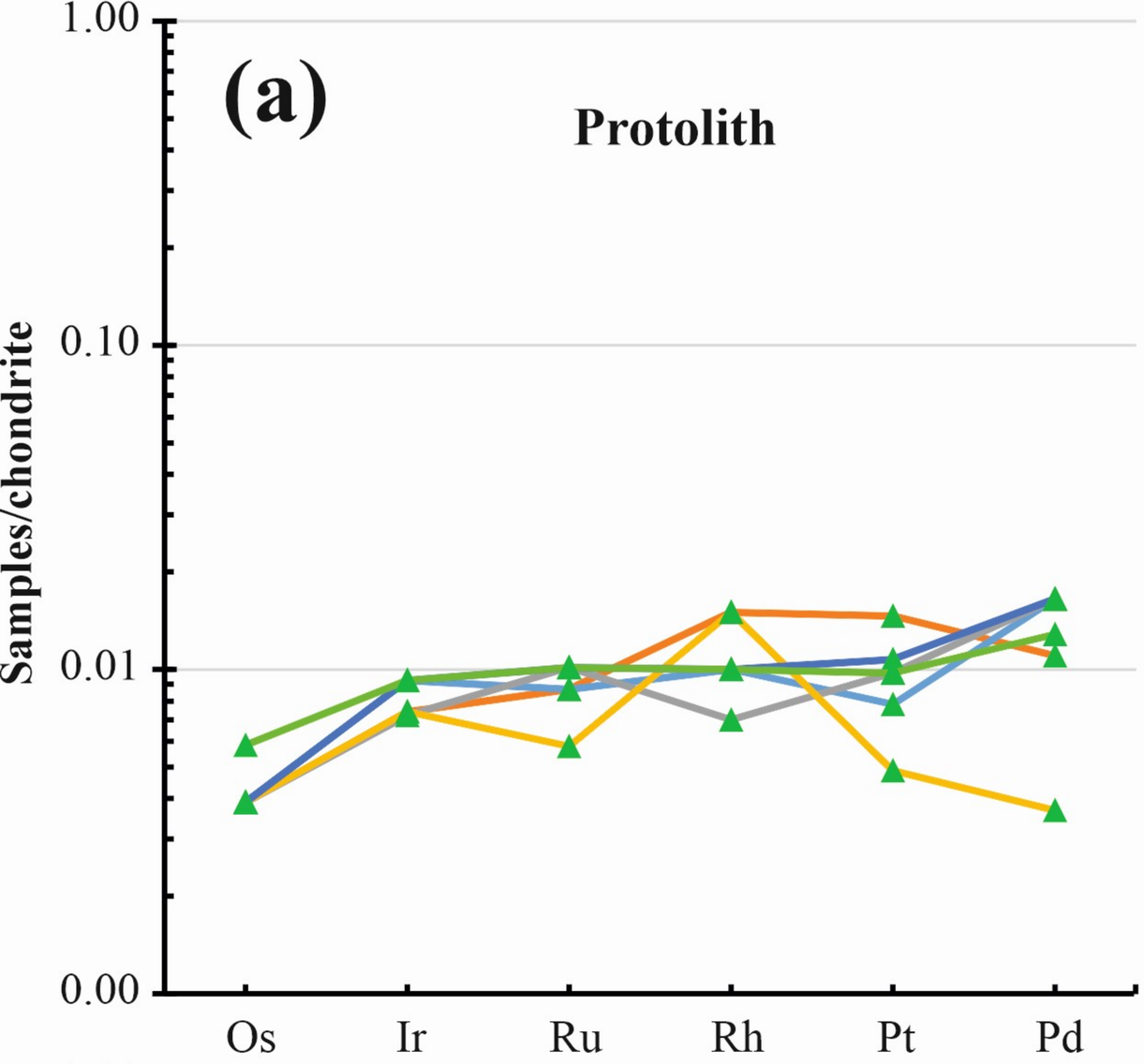
(a)
Protolith
1.00
0.10
0.01
0.00
Samples/chondrite
Os
Ir
Ru
Rh
Pt
Pd

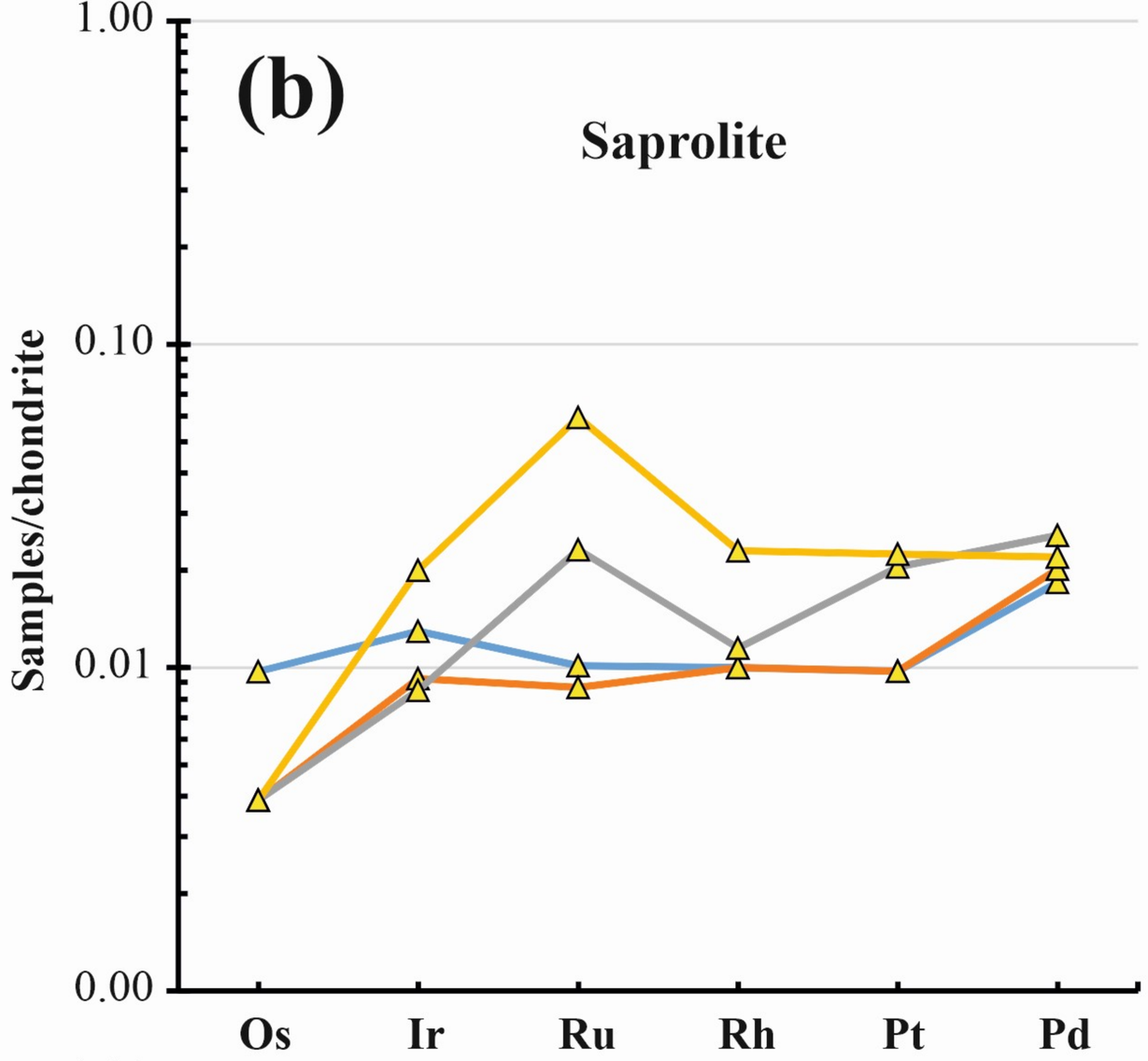
(b)
Saprolite
1.00
0.10
0.01
0.00
Samples/chondrite
Os
Ir
Ru
Rh
Pt
Pd

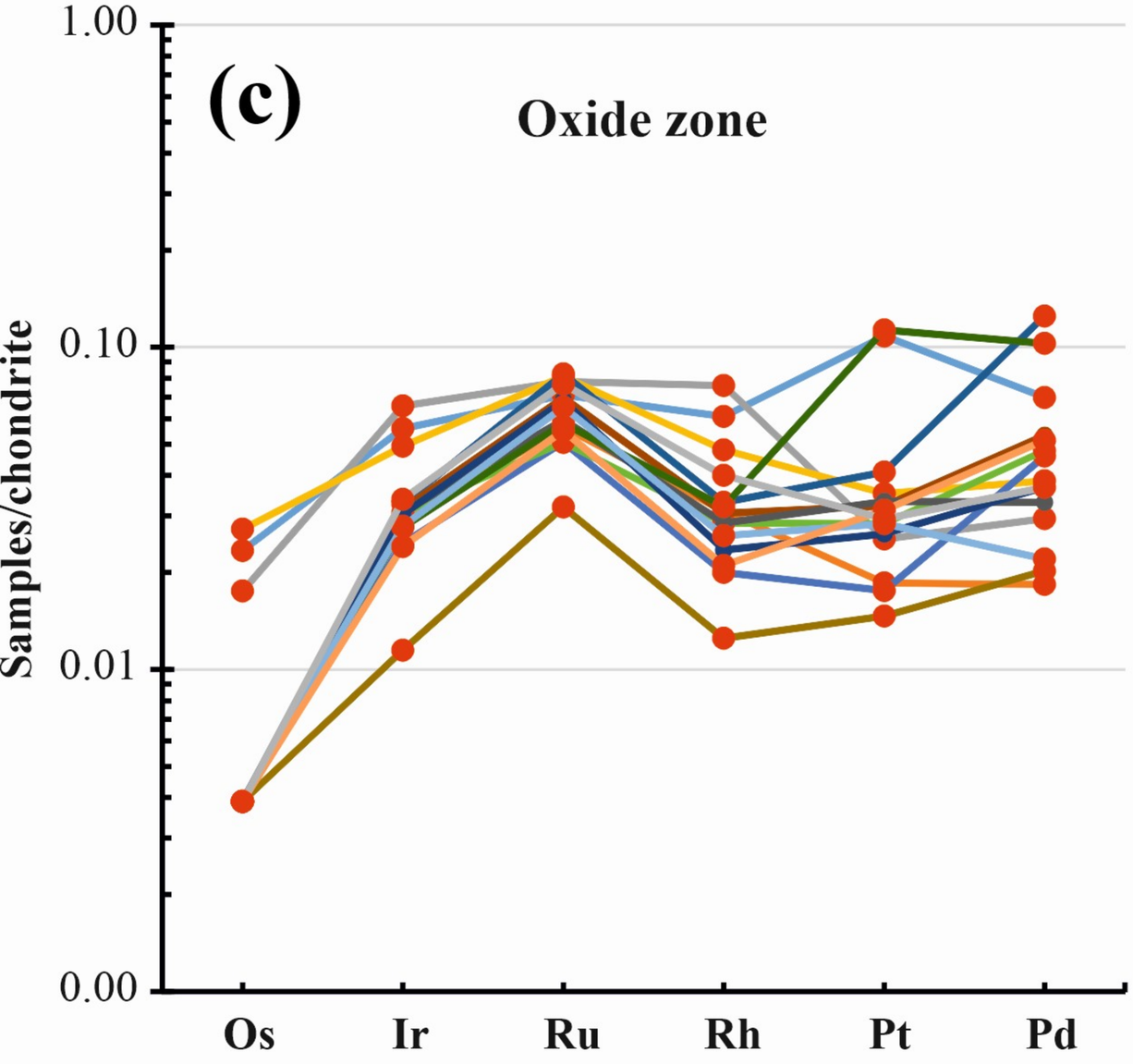
(c)
Oxide zone
1.00
0.10
0.01
0.00
Samples/chondrite
Os
Ir
Ru
Rh
Pt
Pd

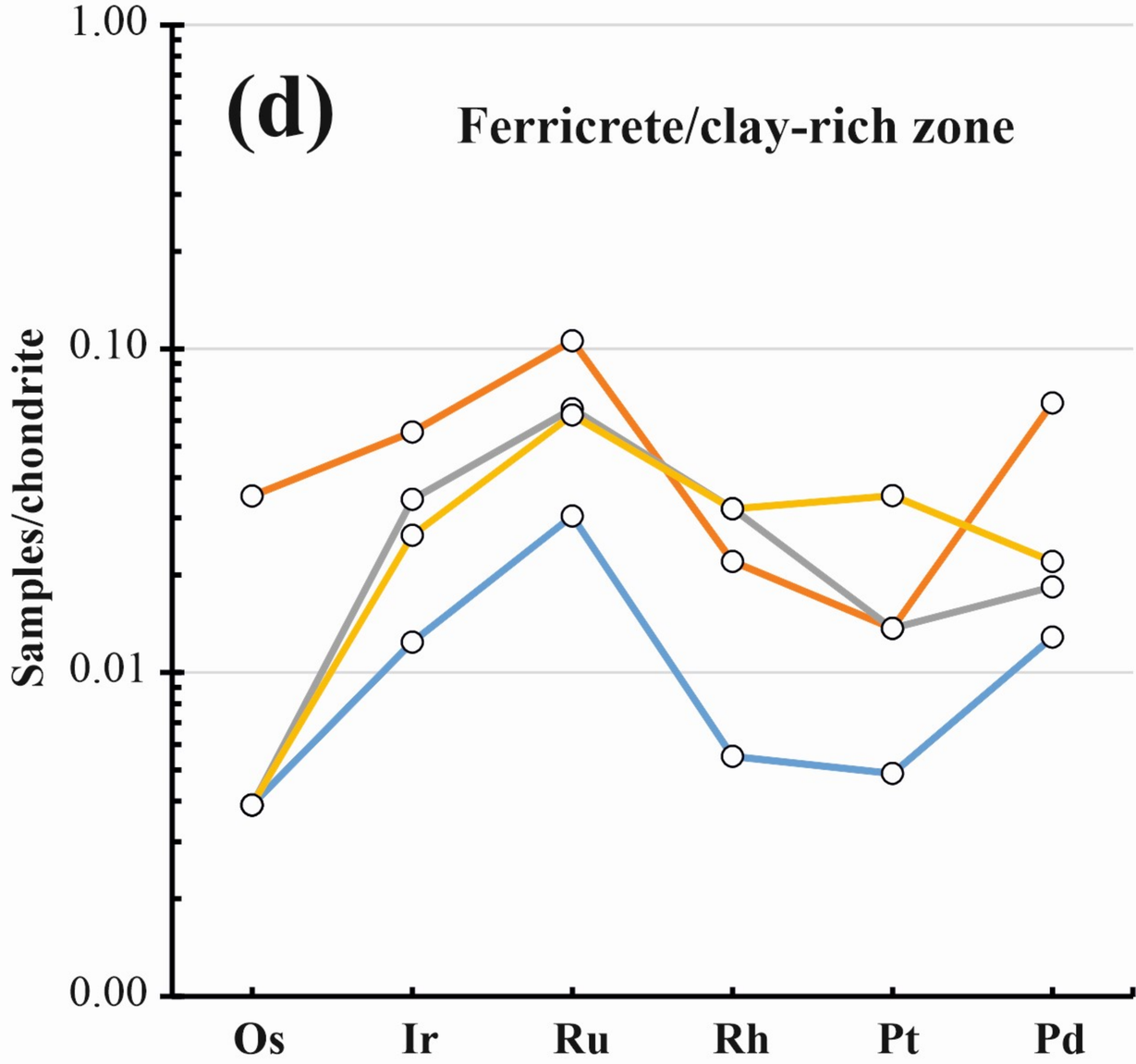
(d)
Ferricrete/clay-rich zone
1.00
0.10
0.01
0.00
Samples/chondrite
Os
Ir
Ru
Rh
Pt
Pd

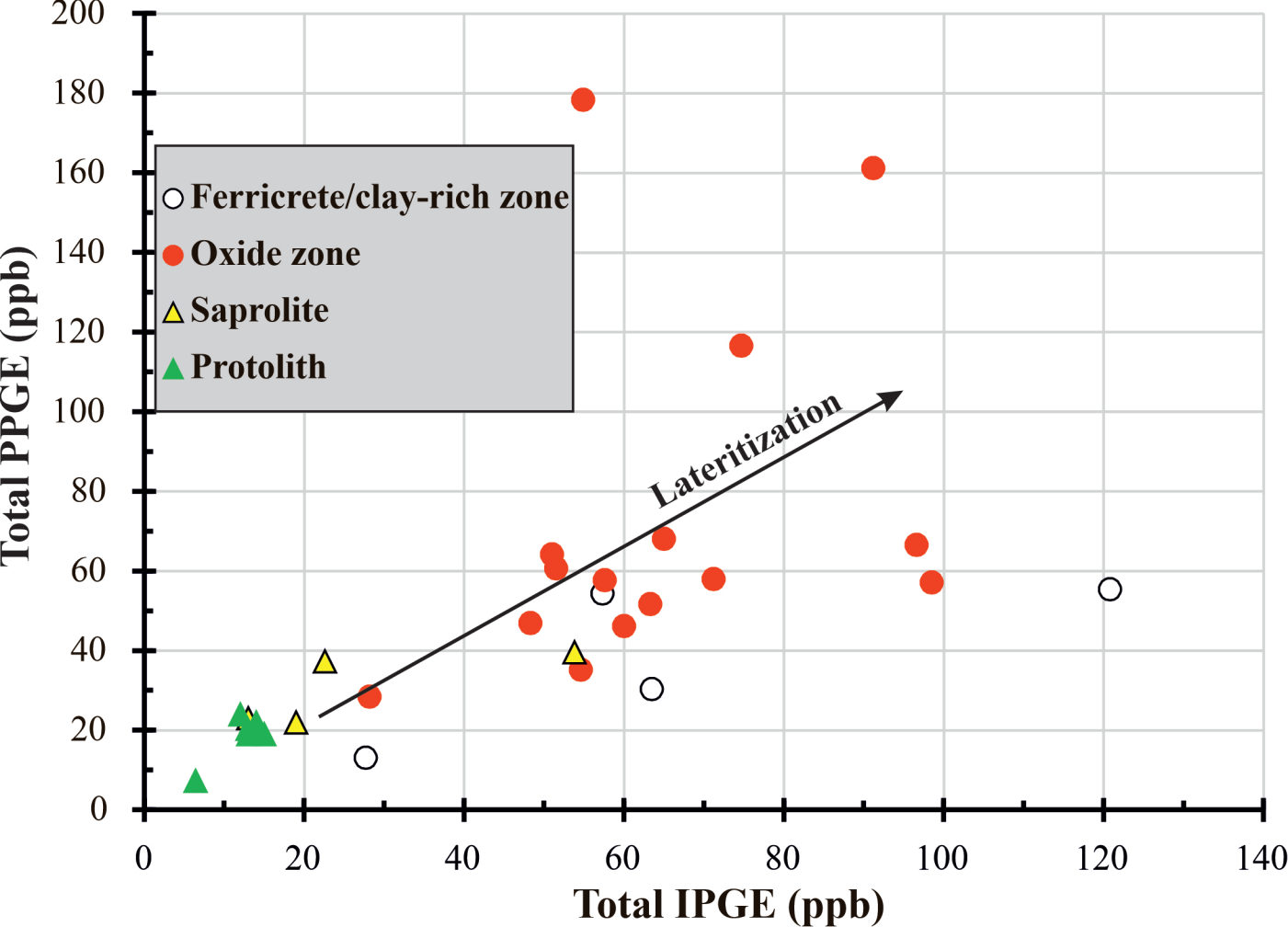
Ferricrete/clay-rich zone
Oxide zone
Saprolite
Protolith
Lateritization
Total PPGE (ppb)
Total IPGE (ppb)
0
20
40
60
80
100
120
140
160
180
200

Ultramafic Index of Alteration (UMIA)
(molar %)

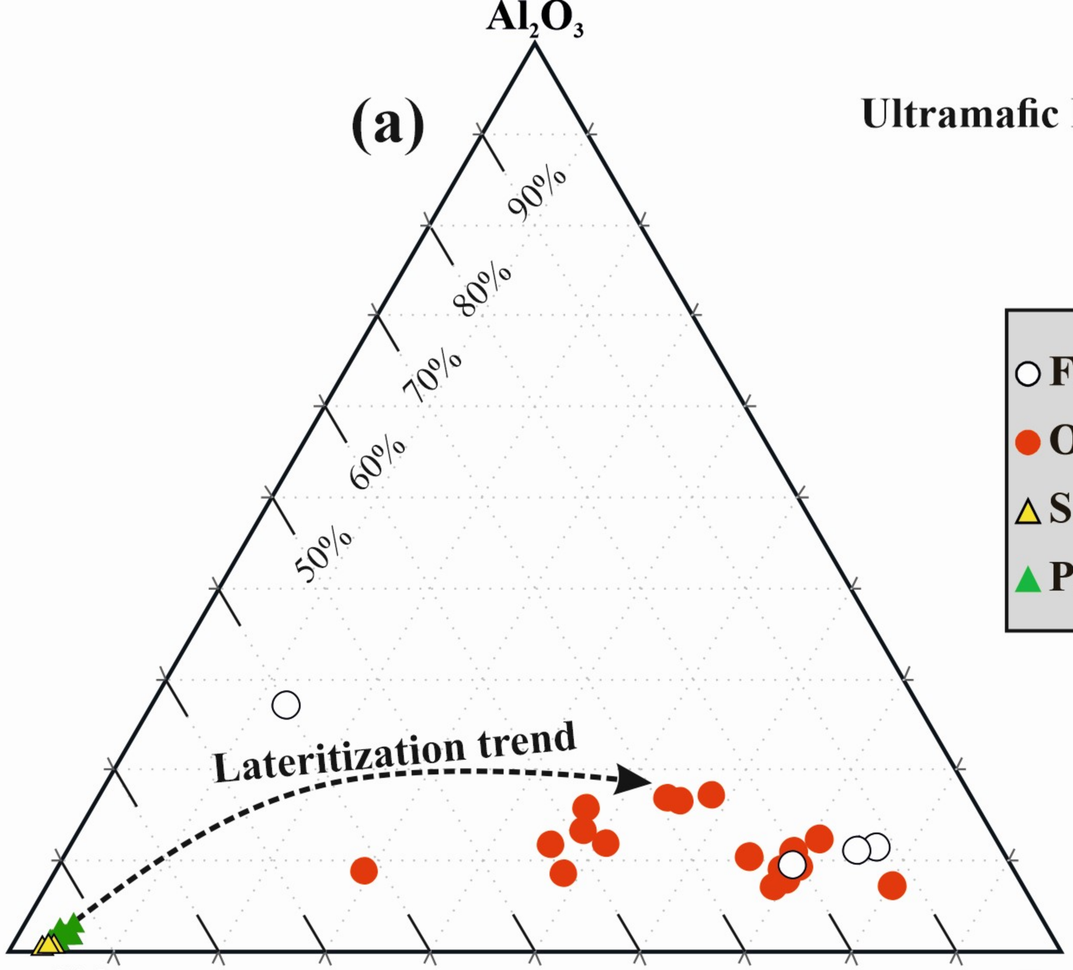

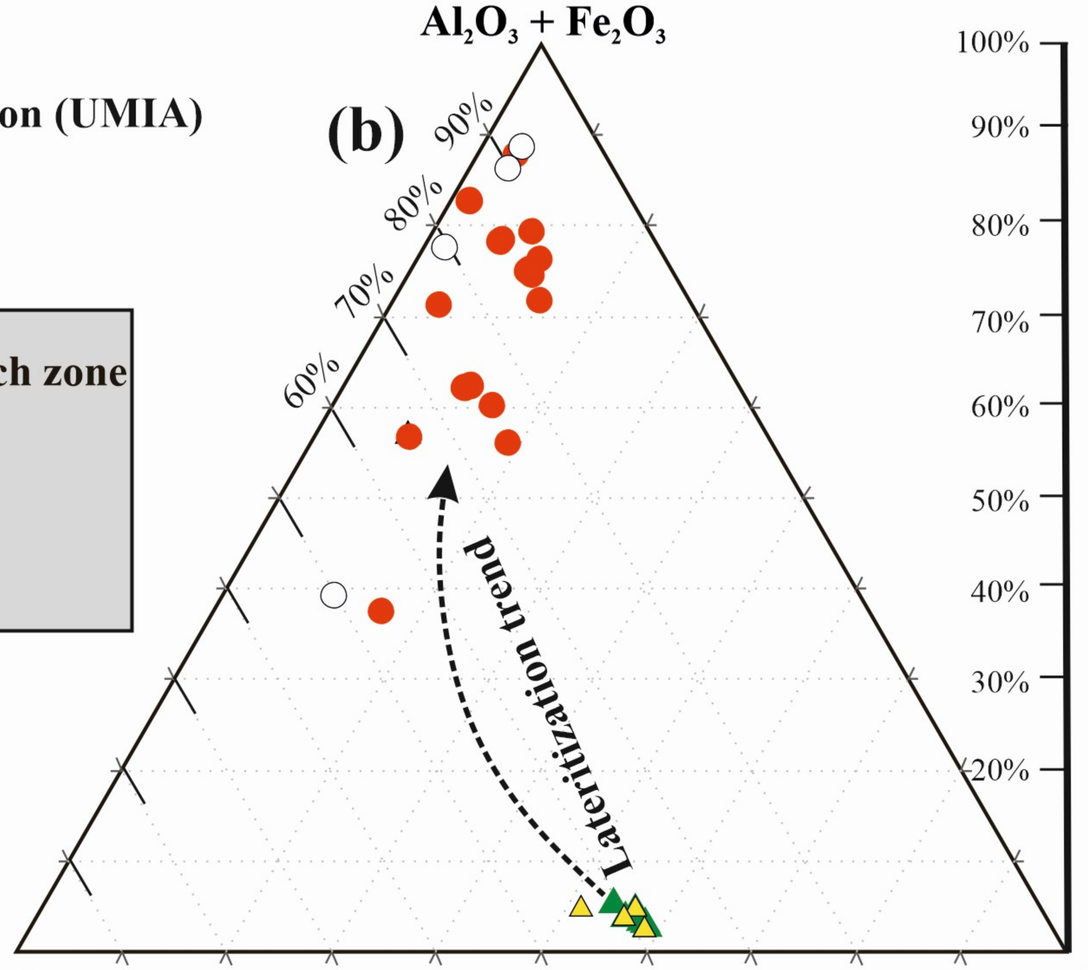

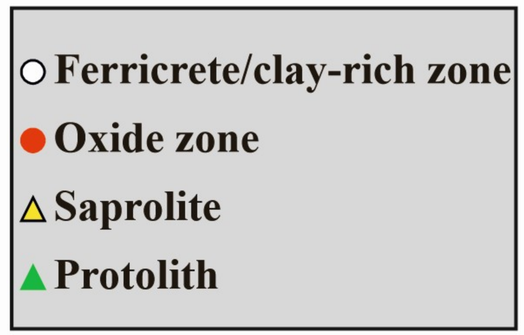

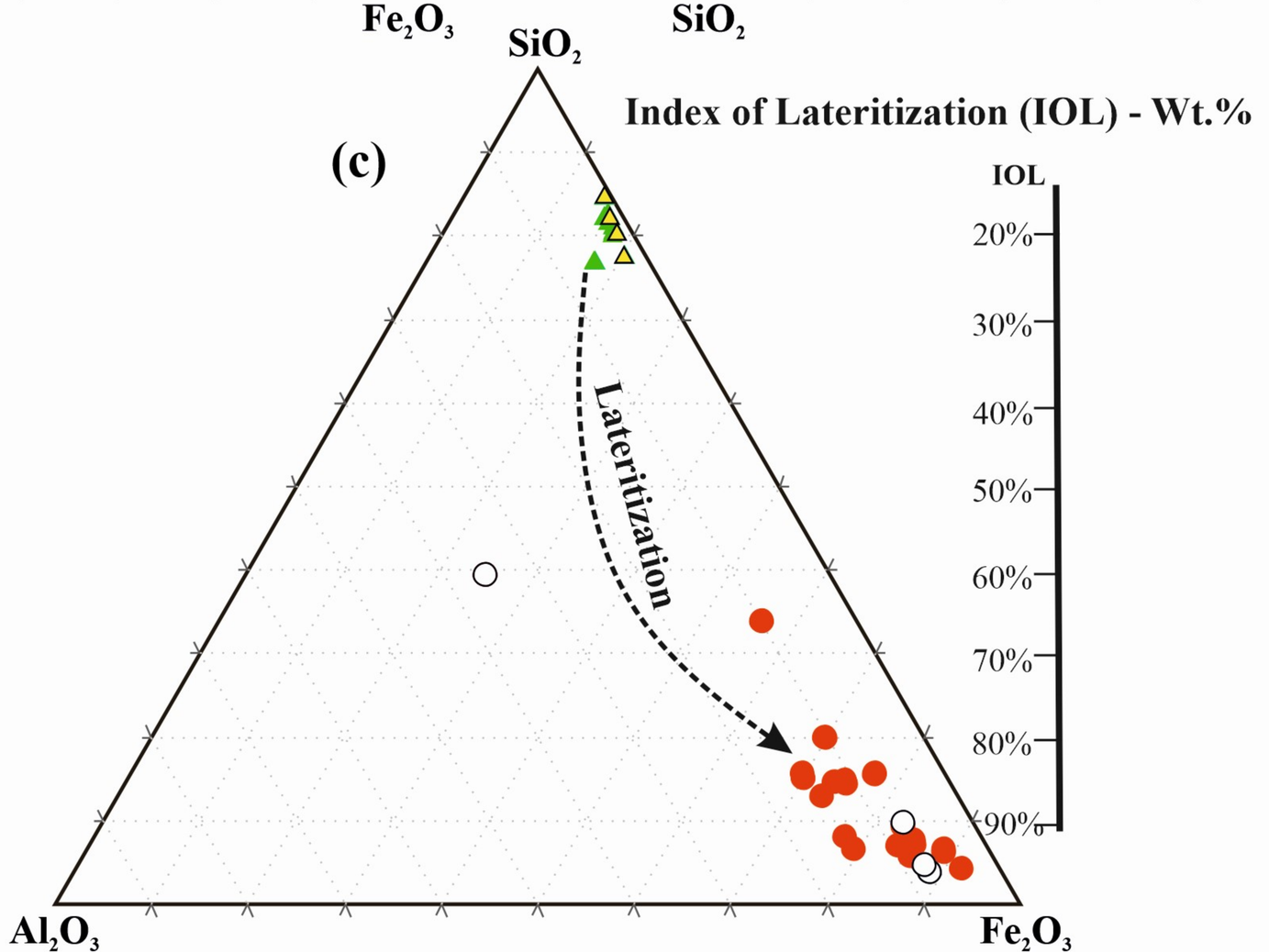

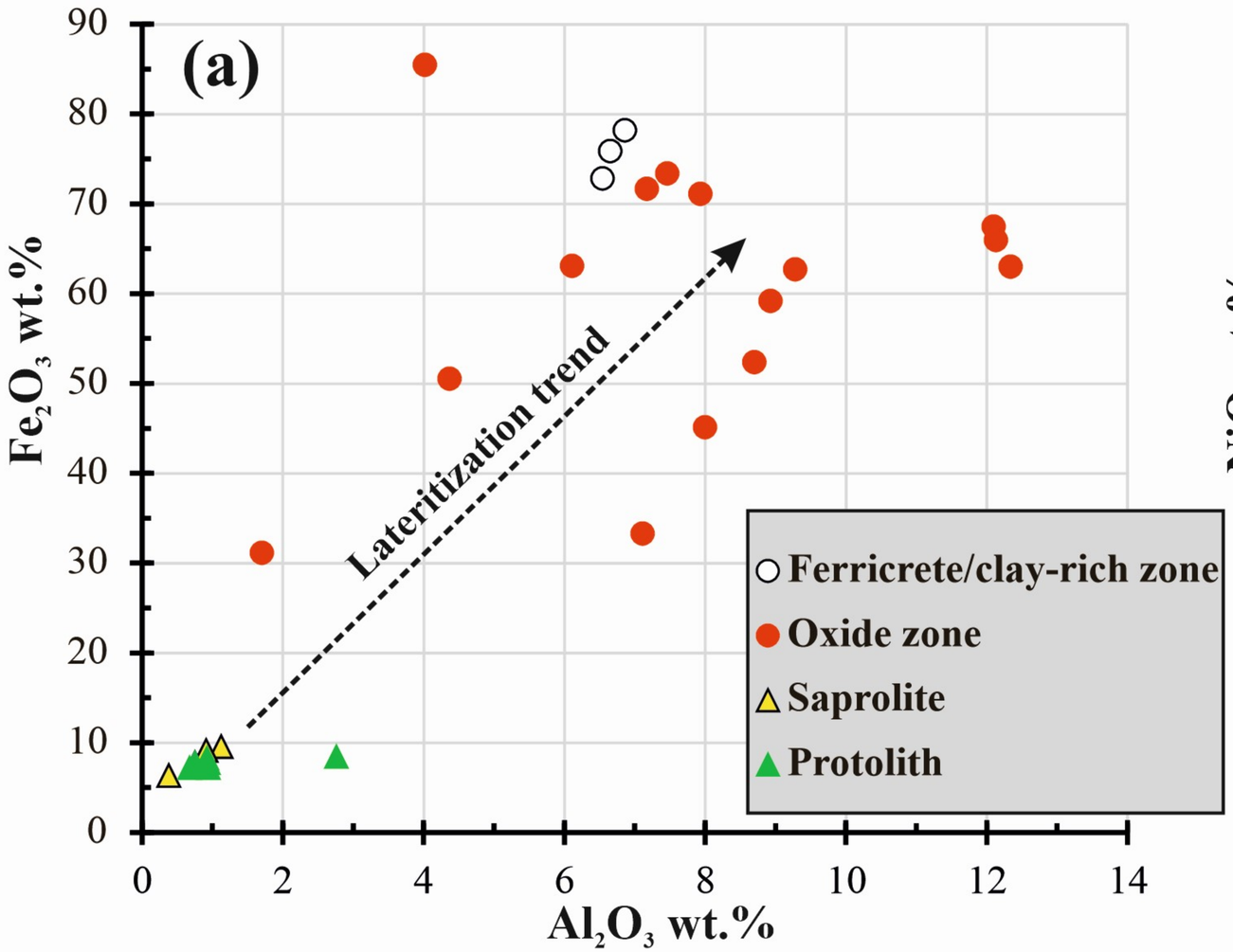
(a)
Fe_2O_3 wt.%
Al_2O_3 wt.%
Lateritization trend
Ferricrete/clay-rich zone
Oxide zone
Saprolite
Protolith

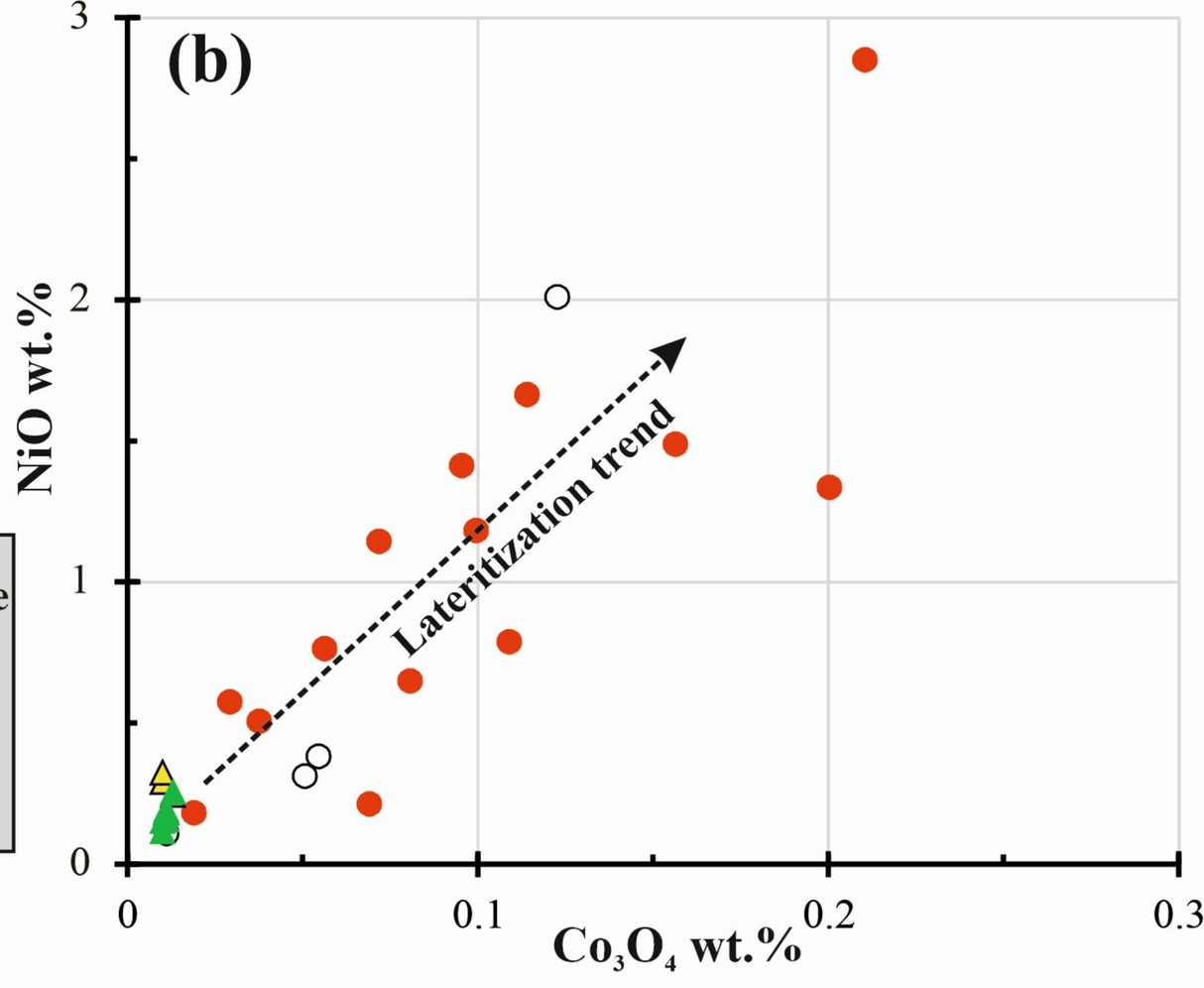
(b)
NiO wt.%
Co_3O_4 wt.%
Lateritization trend

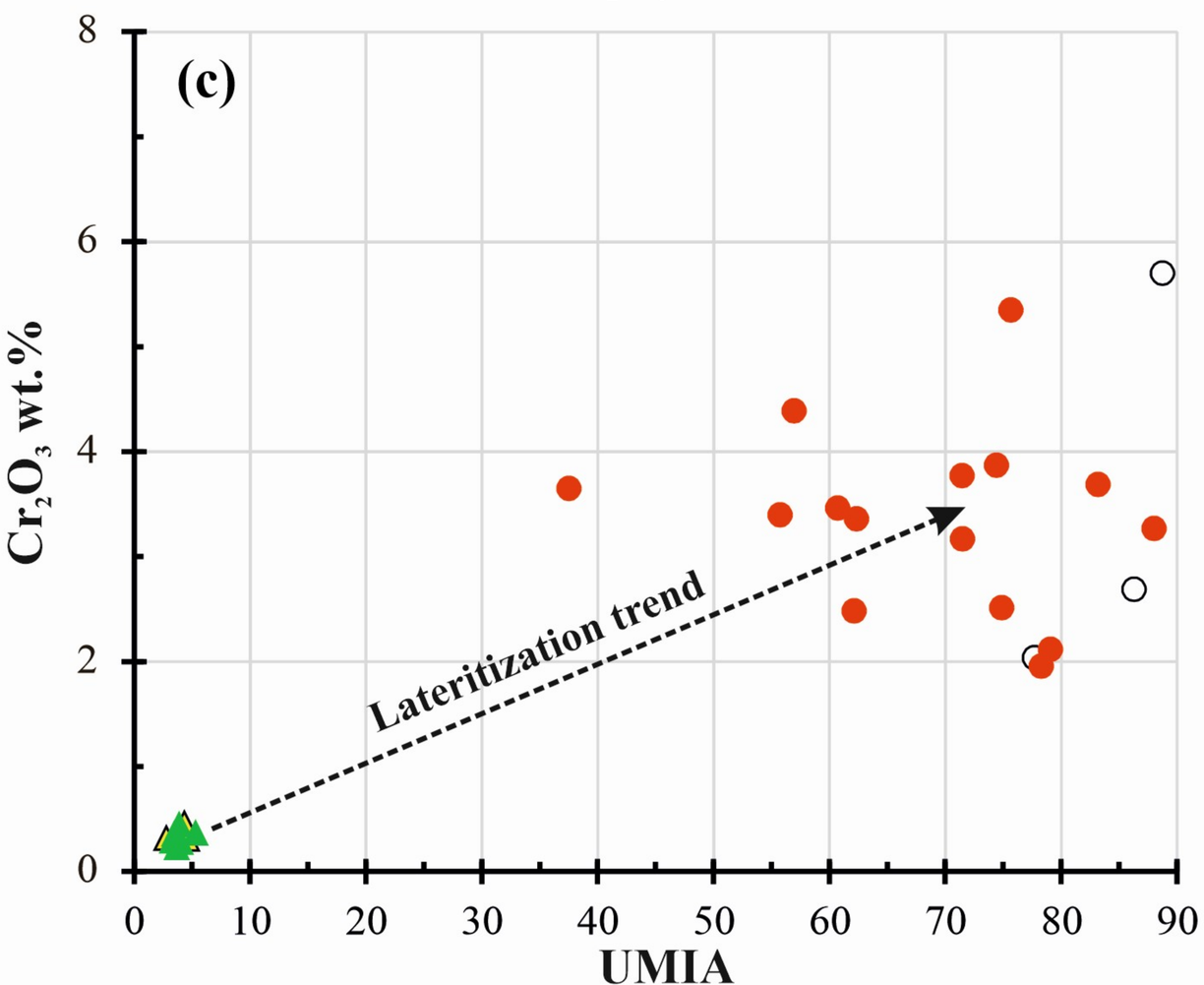
(c)
Cr_2O_3 wt.%
UMIA
Lateritization trend

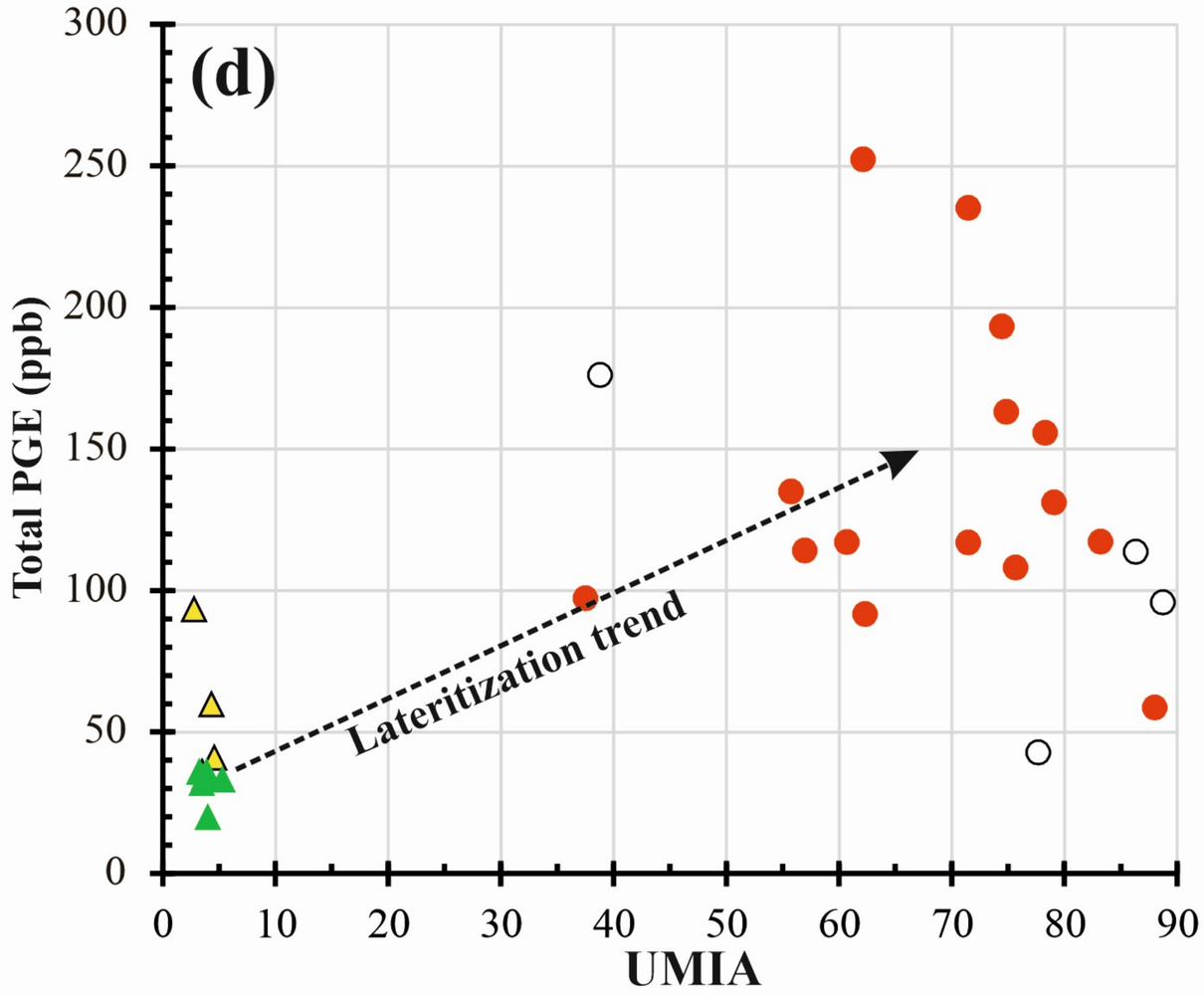
(d)
Total PGE (ppb)
UMIA
Lateritization trend

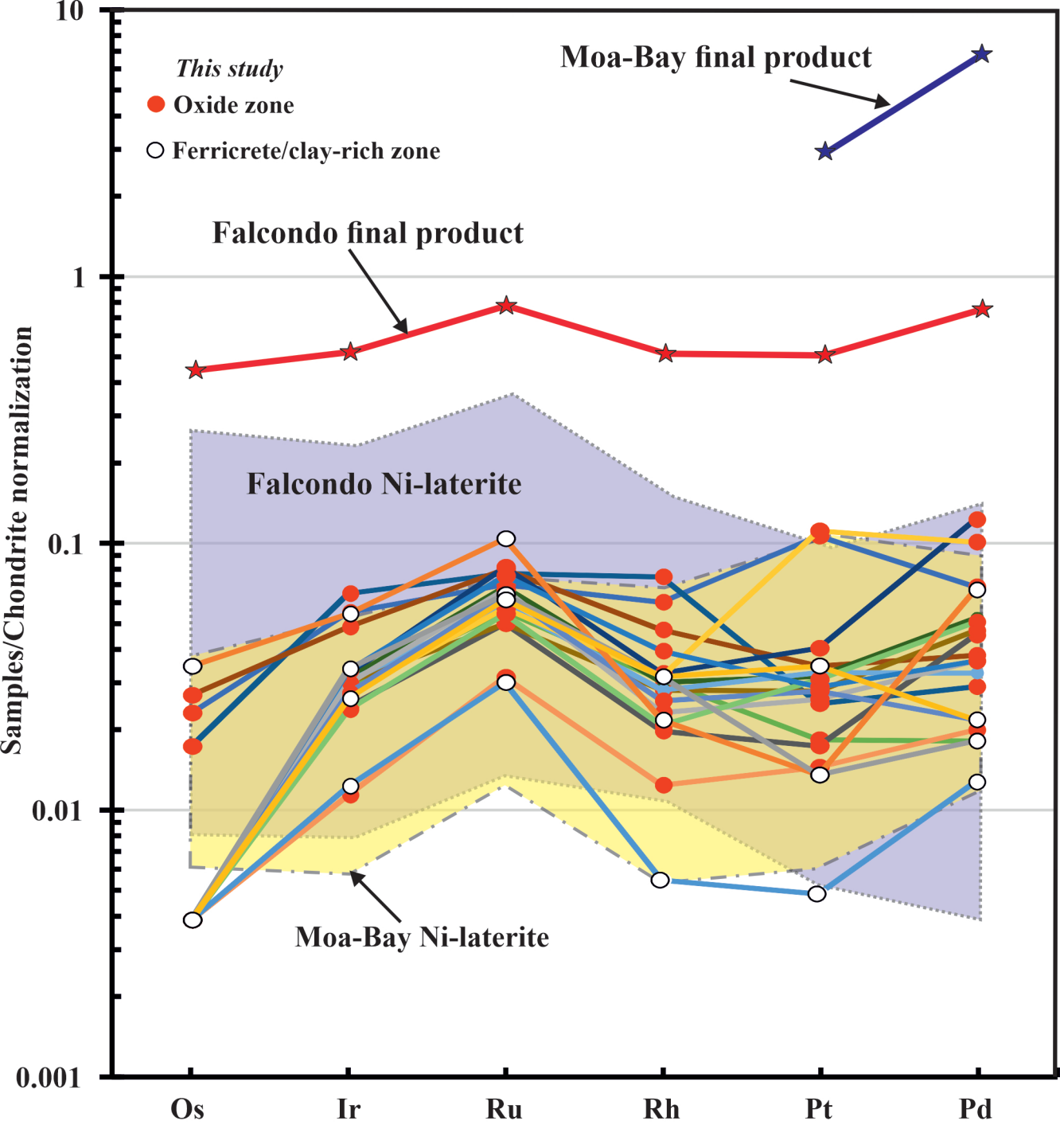
10
1
0.1
0.01
0.001
Samples/Chondrite normalization
This study
Oxide zone
Ferricrete/clay-rich zone
Moa-Bay final product
Falcondo final product
Falcondo Ni-laterite
Moa-Bay Ni-laterite
Os
Ir
Ru
Rh
Pt
Pd

Table 1: Major, selected trace elements composition (wt.%), and PGE contents (ppb) of the protolith
UMIA = Ultramafic Index of Alteration. IOL - Index of Lateritization.

Profile#	loc-1		loc-2	loc-3 and 4	loc-5	loc-6	loc-1
Zone	Protolith		Protolith	Protolith	Protolith	Protolith	saprolite
SiO2	37.67	37.11	37.17	38.21	37.11	36.12	36.74
Al2O3	0.92	0.94	2.76	0.94	0.67	0.75	1.12
Fe2O3(T)	8.28	7.21	8.46	7.77	7.22	7.77	9.60
MnO	0.16	0.13	0.20	0.10	0.10	0.12	0.12
MgO	35.78	36.57	32.87	38.47	37.63	35.16	35.33
CaO	1.60	0.58	2.82	0.08	0.05	0.67	0.68
Na2O	n.d.	n.d.	0.01	n.d.	n.d.	0.02	n.d.
K2O	0.01	0.02	0.02	n.d.	0.00	0.09	0.01
TiO2	0.02	0.02	0.08	0.02	0.01	0.01	0.03
P2O5	0.01	0.01	n.d.	0.05	n.d.	0.00	n.d.
Cr2O3	0.45	0.36	0.37	0.28	0.29	0.23	0.31
NiO	0.16	0.15	0.12	0.26	0.18	0.19	0.18
Co3O4	0.01	0.01	0.01	0.01	0.01	0.01	0.01
LOI	15.72	16.18	15.67	14.72	15.20	15.10	15.81
Total	100.79	99.29	100.56	100.91	98.48	96.25	99.95
UMIA	4	3	5	4	3	4	5
IOL	4	3	5	4	3	4	5
PGE (ppb)							
Os	2	2	2	2	2	3	5
Ir	4	5	4	0.4	5	5	7
Ru	6	6	7	4	7	7	7
Rh	3	2	1	0.3	2	2	2
Pt	15	8	10	5	11	10	10
Pd	6	9	9	2	9	7	10
Au	n.d.	n.d.	3	1.4	n.d.	n.d.	n.d.
∑ PGE	36	32	33	14	36	34	41
∑ IPGE	12	13	13	6	14	15	19
∑ PPGE	24	19	20	7	22	19	22
Pd/IrN	1.49	1.78	2.18	4.95	2.29	1.78	1.42
Ru/PtN	0.59	1.11	0.89	1.48	1.04	0.95	1.04

and saprolite samples of the studied Ni-laterite profiles of the Oman ophiolite.

loc-2 saprolite	loc-3 and 4 saprolite	
38.96	40.66	36.92
0.75	0.91	0.38
7.78	9.16	6.39
0.11	0.12	0.09
36.43	31.91	37.00
0.76	1.19	3.25
0.01	0.01	0.01
0.01	0.03	0.01
0.01	0.02	0.01
0.01	0.05	0.04
0.35	0.46	0.32
0.29	0.33	0.25
0.01	0.02	0.01
14.60	15.88	15.86
100.09	100.74	100.54
3	4	3
4	4	3
2	2	2
5	5	11
6	16	41
2	2	5
10	21	23
11	14	12
n.d.	5	1
36	60	93
13	23	54
23	37	40
1.39	3.02	1.10
1.04	1.13	2.65

Table 2: Major, selected trace elements composition (wt.%), and PGE contents of the oxide and clay-rich zone UMIA = Ultramafic Index of Alteration. IOL - Index of Lateritization.

Profile#	loc-1						loc
Zone	oxide zone				ferricrete/clay-rich		oxide
SiO2	7.32	12.24	4.35	2.23	8.42	27.06	26.93
Al2O3	7.11	9.28	4.37	1.70	6.54	24.49	8.00
Fe2O3(T)	33.31	62.70	50.53	31.14	72.82	16.82	45.14
MnO	0.54	0.18	0.65	2.52	0.18	0.18	0.46
MgO	1.93	3.57	1.10	1.37	0.37	3.80	6.18
CaO	24.30	1.33	18.59	30.31	0.20	1.30	0.61
Na2O	0.06	0.06	0.04	0.21	0.10	0.14	0.06
K2O	0.02	0.03	0.01	0.01	0.01	0.84	0.05
TiO2	0.08	0.09	0.06	0.03	0.11	0.57	0.21
P2O5	0.04	0.01	0.01	0.01	0.03	0.01	0.01
Cr2O3	2.48	3.36	1.96	2.51	2.04	11.44	3.65
NiO	0.51	1.49	0.58	1.14	0.38	2.01	1.41
Co3O4	0.04	0.16	0.03	0.07	0.05	0.12	0.10
LOI	22.41	6.37	16.67	25.62	8.02	12.59	7.11
Total	100.15	100.86	98.94	98.88	99.28	101.37	99.92
UMIA	62	62	78	75	78	39	38
IOL	74	71	86	80	86	53	41
PGE (ppb)							
Os	12	2	9	14	2	18	2
Ir	30	16	36	27	7	30	13
Ru	49	39	54	56	21	73	35
Rh	12	6	15	10	1	4	4
Pt	111	19	26	36	5	14	18
Pd	38	10	16	21	7	37	25
Au	2	2	4	3	1	15	3
∑ PGE	252	92	156	163	43	176	97
∑ IPGE	91	57	99	97	30	121	50
∑ PPGE	161	35	57	67	13	55	47
Pd/IrN	1.25	0.64	0.45	0.78	1.04	1.23	1.86
Ru/PtN	0.66	3.05	3.09	2.31	6.24	7.75	2.89

samples of the studied Ni-laterite profiles of the Oman ophiolite.

c-2	loc-3 and 4		loc-5				
zone	oxide zone		oxide zone			ferricrete/clay-rich	
16.62	6.14	12.55	5.75	3.67	10.84	3.08	4.01
8.93	7.17	6.11	7.93	4.02	12.34	6.65	6.86
59.20	71.69	63.11	71.13	85.50	63.02	75.87	78.18
0.31	0.26	0.19	0.10	0.04	0.11	0.05	0.12
2.81	3.07	6.14	0.40	0.69	1.03	0.70	0.87
0.39	0.47	0.32	0.06	0.07	0.29	0.51	0.92
0.05	0.01	0.01	0.45	0.01	0.09	0.08	0.20
0.02	0.02	0.03	0.10	0.01	0.01	0.01	0.01
0.19	0.06	0.26	0.24	0.11	0.11	0.13	0.17
0.03	0.06	0.05	0.12	0.08	0.06	0.09	0.06
4.39	3.87	3.40	3.69	3.27	3.77	5.70	2.69
0.79	1.67	1.85	0.21	0.18	0.76	0.11	0.31
0.11	0.11	0.50	0.07	0.02	0.06	0.01	0.05
4.99	5.17	6.06	10.42	3.23	10.67	10.46	4.87
98.83	99.77	100.58	100.67	100.90	103.16	103.45	99.32
57	74	56	83	88	71	89	86
64	83	60	95	94	86	99	96
2	2	2	2	2	2	2	2
17	18	17	17	6	16	19	14
35	57	48	41	22	47	45	43
6	7	6.1	6	3	5	6	6
29	42	33	34	15	27	14	36
26	68	29	18	11	20	10	12
2	8.6	0.8	3	3	1	1	1
114	193	135	117	59	117	96	114
54	77	67	60	30	65	66	59
61	117	68	58	29	52	30	54
1.56	3.81	1.69	1.07	1.76	1.22	0.54	0.83
1.79	2.02	2.16	1.79	2.18	2.59	4.77	1.77

loc-6			
oxide zone			
6.59	5.43	10.20	4.78
12.13	12.10	8.70	7.46
65.99	67.49	52.36	73.39
0.32	0.19	0.17	0.33
4.14	3.37	3.94	2.48
1.88	1.28	6.36	2.81
0.03	0.05	0.17	0.05
0.01	0.01	0.02	0.01
0.16	0.14	0.04	0.07
0.01	0.01	0.01	0.01
3.17	5.35	3.46	2.12
1.18	0.65	2.85	1.34
0.10	0.08	0.21	0.20
4.87	4.27	10.65	4.48
100.58	100.42	99.15	99.53
71	76	61	79
85	91	69	89
2	2	2	2
15	15	13	18
40	45	38	53
6	5	4	8
116	29	32	30
56	12	28	20
1	1	1	1
235	108	117	131
57	62	53	73
178	46	64	58
3.72	0.79	2.13	1.09
0.51	2.31	1.76	2.62